



## Review Article

## SEM petrography of dispersed organic matter in black shales: A review

Bei Liu<sup>a,b,\*</sup>, Maria Mastalerz<sup>c</sup>, Juergen Schieber<sup>b</sup><sup>a</sup> Key Laboratory of Tectonics and Petroleum Resources of Ministry of Education, China University of Geosciences, Wuhan, Hubei 430074, China<sup>b</sup> Department of Earth and Atmospheric Sciences, Indiana University, Bloomington, IN 47405, USA<sup>c</sup> Indiana Geological and Water Survey, Indiana University, Bloomington, IN 47405-2208, USA

## ARTICLE INFO

**Keywords:**  
 Dispersed organic matter  
 Maceral  
 Organic petrography  
 SEM  
 Organic pores  
 Black shale  
 Source-rock reservoir

## ABSTRACT

Organic matter (OM)-hosted pores are important constituents of the pore system of black shales and play a crucial role in determining their methane adsorption capacity and porosity. OM-hosted pores are generally observed and described with scanning electron microscope (SEM) on Ar ion-milled surfaces. However, SEM imaging is not able to reliably distinguish OM types and relate the observed pores to specific macerals. Partly because of this inability to relate organic pores to macerals, the evolution of organic porosity during thermal maturation remains poorly understood.

In this paper, we review the petrographic characteristics of dispersed organic matter (DOM) in black shales under the SEM. Organic petrographic classification of DOM developed for reflected-light microscopy is so far the most practical method when describing DOM in black shales under the SEM because this classification has information on the origin of DOM. Therefore, correlative microscopy (combination of reflected-light and electron microscopy) is the most effective method to identify both OM types and OM-hosted pores. This method, however, is not readily available to most researchers. Although identifying OM on the basis of SEM observations is a challenging task, it is achievable provided there is a good understanding of the studied shales, especially their thermal maturity and original OM composition. Therefore, the overall objective of this paper is to review petrographic characteristics of DOM in black shales under the SEM to provide some guidelines for identifying DOM from SEM observations.

We also review factors that control the formation and preservation of OM-hosted pores. OM-hosted pores consist of primary and secondary organic pores. Primary organic pores are pores inherited from the biological structure of the original OM. Secondary organic pores develop during hydrocarbon generation and expulsion from oil-prone OM and are hosted by solid bitumen or pyrobitumen. The development of secondary organic pores is controlled by thermal maturity and OM type, and their preservation is subject to thermal maturity, OM content, and mineralogical composition.

The presented view of the evolution of micropore and mesopore characteristics of OM with thermal maturity is based on data from the literature. The specific surface area and pore volume of OM in black shales follow parabolic patterns with increasing thermal maturity (quantified via vitrinite reflectance,  $R_o$ ). The initial increase reflects development of OM-hosted pores, and the subsequent decrease is due to denser stacking of aromatic units in the macromolecular structure of OM, with maximum values (specific surface area  $\sim 300 \text{ m}^2/\text{g}$  and pore volume  $\sim 0.3 \text{ cm}^3/\text{g}$ ) reached at  $R_o$  values in the 2.5–3.5% range. The contribution of OM-hosted pores to the pore characteristics of black shales depends on OM content, OM type, and thermal maturity.

## 1. Introduction

Organic matter (OM) quantity, quality, and thermal maturity are key parameters in evaluation of both conventional and unconventional petroleum systems (Tissot and Welte, 1984; Peters and Cassa, 1994; Curtis,

2002; Passey et al., 2010; Jarvie, 2012a, 2012b; Hackley and Cardott, 2016). OM in black shales serves as both the source of oil and gas and the storage space for them in unconventional petroleum systems, which makes black shales self-sourced hydrocarbon reservoirs (Curtis, 2002; Passey et al., 2010; Jarvie, 2012a, 2012b; Cardott et al., 2015; Qiu and

\* Corresponding author at: Key Laboratory of Tectonics and Petroleum Resources of Ministry of Education, China University of Geosciences, Wuhan, Hubei 430074, China.

E-mail address: [liubeicugb@outlook.com](mailto:liubeicugb@outlook.com) (B. Liu).

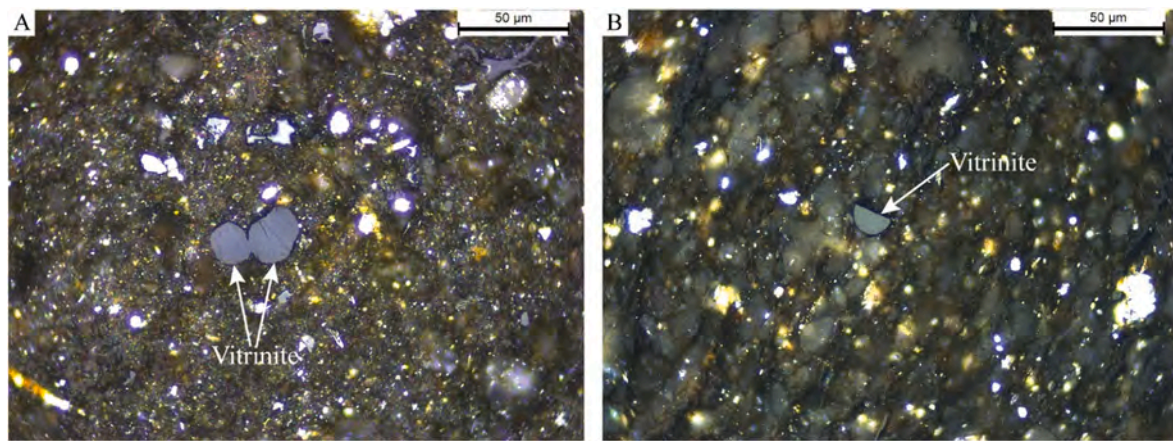


**Fig. 1.** Photomicrographs of vitrinite in reflected white light and oil immersion. Core samples of the New Albany Shale from Daviess County, IN ( $R_o$  0.55%).

Zou, 2020). OM-hosted pores make significant contributions to the pore network of tight shale reservoirs (Loucks et al., 2009, 2012; Schieber, 2010, 2013; Curtis et al., 2011; Mastalerz et al., 2013; Schieber et al., 2016; İnan et al., 2018; Katz and Arango, 2018; Ko et al., 2018) and critically control the gas content and methane adsorption capacity of black shales (Ross and Bustin, 2009; Hao et al., 2013; Mastalerz et al., 2016a; Qiu et al., 2020a).

Scanning electron microscopes (SEM) are commonly used to image OM-hosted pores in black shales (e.g., Loucks et al., 2009, 2012; Schieber, 2010; Kwiecińska et al., 2019). An important disadvantage of SEM imaging, however, is its inability to distinguish OM types, because all OM appears black under the SEM due to a low density (Camp, 2016; Kwiecińska et al., 2019; Valentine and Hackley, 2019). OM types (macerals) are best identified with reflected-light microscopy based on colour, reflectance, form, and fluorescence, and this technique has been used to identify OM in coals (Taylor et al., 1998; Suárez-Ruiz et al., 2012) and dispersed organic matter (DOM) in shales (Potter et al., 1998; Hackley and Cardott, 2016; Flores and Suárez-Ruiz, 2017; Mastalerz et al., 2018) for decades. Correlative reflected-light and electron microscopy combines the advantages of both techniques and has been successfully used in some shale sequences (Hackley et al., 2017; Liu et al., 2017; Valentine and Hackley, 2019; Hackley et al., 2021; Wei et al., 2021). However, because this approach requires a combination of skills and instrumentation that is not always available, we propose a strategy that facilitates reliable identification of OM types under the SEM. Accurate identification of OM types under the SEM will help in the evaluation of the thermal evolution of DOM and improve the understanding of the role of OM-hosted pores in source-rock reservoirs.

The purpose of this paper is to provide a review of DOM in black shales and their petrographic characteristics under the SEM. We hope this review will: a) help researchers (e.g., sedimentologists or SEM petrographers) who have no access to organic petrographic technique to more reliably identify the types of DOM and relate them to OM-hosted pores in unconventional shale reservoirs; b) uncover the evolution of OM-hosted pores during thermal maturation, and c) provide some OM-related insights into characterization of tight shale reservoirs and exploitation of hydrocarbon resources in black shale successions.

## 2. Organic petrographic classification of dispersed organic matter in black shales

The organic petrographic classification of DOM in black shales (e.g., Stasiuk et al., 2002; Flores and Suárez-Ruiz, 2017; Mastalerz et al., 2018) is an extension of the organic petrographic classification of OM in coals (ICCP, 1998; 2001; Taylor et al., 1998; Pickel et al., 2017). Hackley and Cardott (2016) and Hackley et al. (2021) provided comprehensive reviews of the application of organic petrography in shale petroleum systems. Organic petrographic classification of DOM in black shales includes five maceral groups, with each group consisting of multiple macerals (Stasiuk et al., 2002; Mastalerz et al., 2018). Of the five groups, vitrinite, inertinite, liptinite, and zooclasts are primary OM (deposited at the same time with mineral matrix), whereas secondary OM is the result of transformation of oil-prone macerals during thermal maturation.

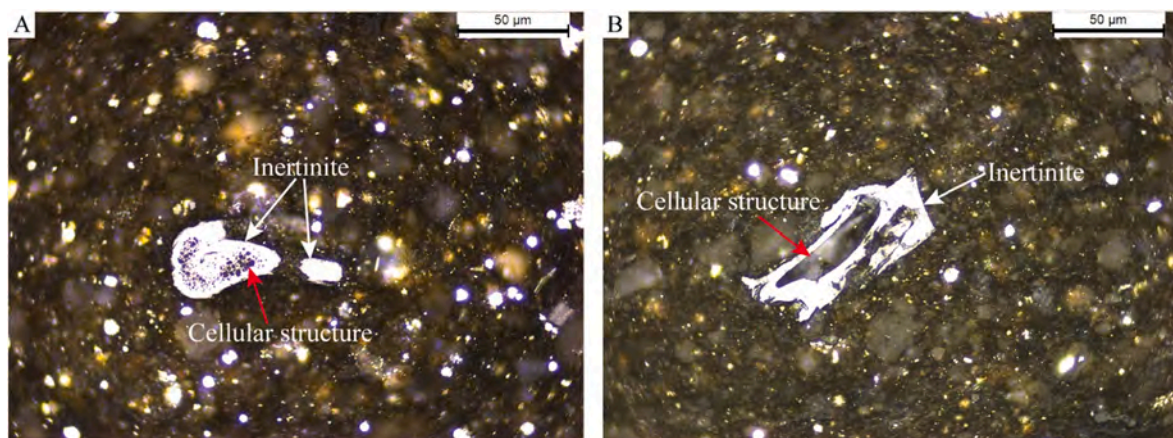


**Fig. 2.** Photomicrographs of inertinite in reflected white light and oil immersion. Core samples of the New Albany Shale from Daviess County, IN ( $R_o$  0.55%).

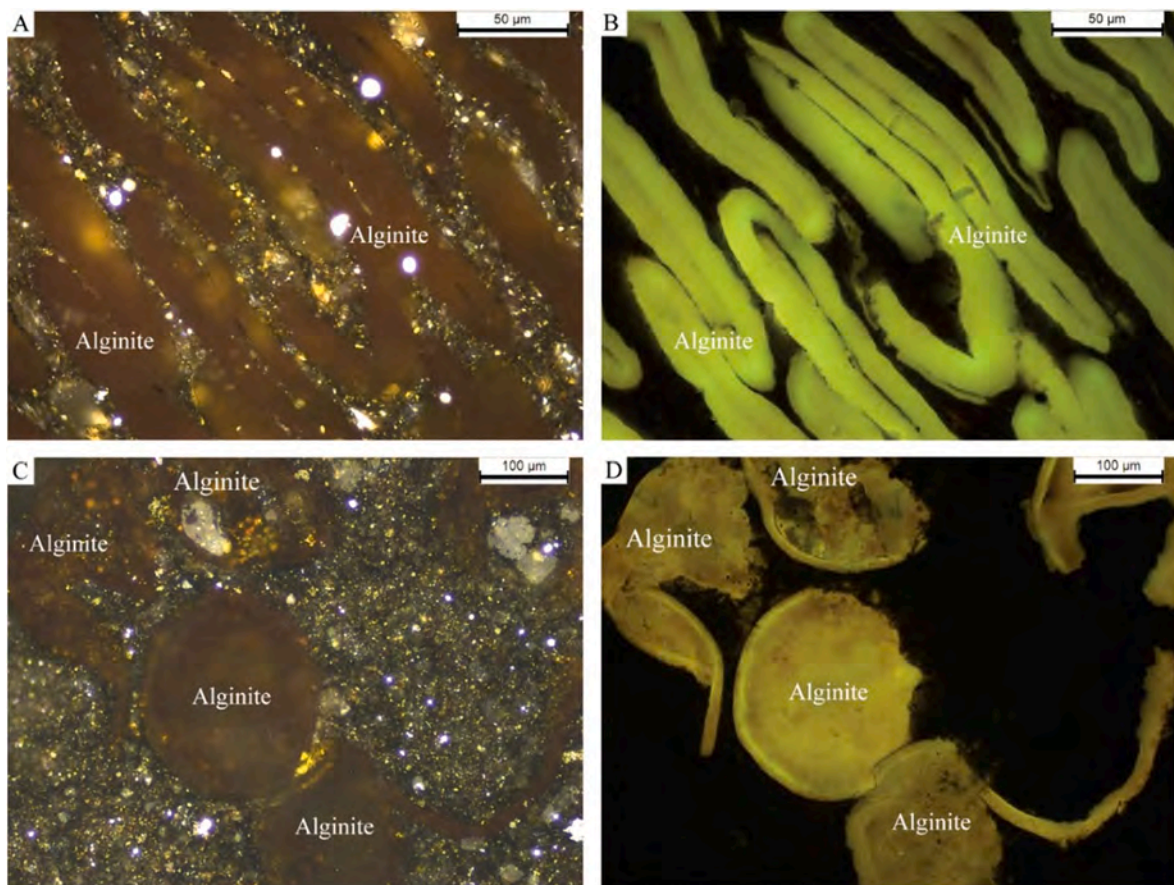


**Fig. 3.** Photomicrographs of alginite derived from *Tasmanites* cysts in reflected white light and oil immersion (A, C) and in fluorescence mode (B, D). (A, B) Core sample of the New Albany Shale from Daviess County, IN ( $R_o$  0.55%). (C, D) Core sample of the New Albany Shale from Pike County, IN ( $R_o$  0.73%). Note that alginite in panel D with a higher maturity shows more yellowish fluorescence than that in panel B. A and B = perpendicular to bedding; C and D – parallel to bedding.

## 2.1. Vitrinite

Vitrinite in coals and shales is derived from terrigenous higher plants (Taylor et al., 1998). It has low oil generation potential and high potential for methane generation. Vitrinite-rich OM is typically type III kerogen (Peters and Cassa, 1994). The reflectance of vitrinite ( $R_o$ ) is commonly used to indicate the thermal maturity of host rocks such as coals and black shales (Mukhopadhyay, 1994; Liu et al., 2020b).  $R_o$

increases with thermal maturity because the degree of aromatization and condensation of the macromolecular structure of vitrinite increases with temperature, which increases the reflectivity of vitrinite (McCartney and Teichmüller, 1972).  $R_o$  is unsuitable as a thermal maturity indicator in pre-Devonian rocks (Buchardt and Lewan, 1990; Schleicher et al., 1998; Petersen et al., 2013; Reyes et al., 2018) because of the lack of organic debris from land-derived vascular plants prior to the Devonian (Kenrick and Crane, 1997).

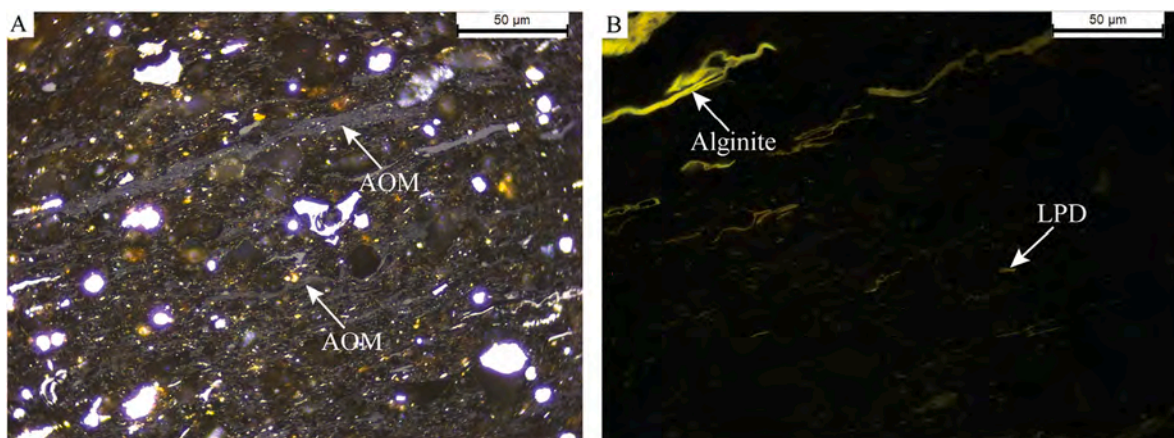


**Fig. 4.** Photomicrographs of amorphous organic matter (AOM) in reflected white light and oil immersion (A) and in fluorescence mode (B). AOM appears structureless and occurs as organic streaks parallel to bedding. It shows no fluorescence. In comparison, alginite has distinct algal bodies and shows strong greenish yellow fluorescence. Core sample of the New Albany Shale from Daviess County, IN ( $R_o$  0.55%). LPD = liptodetrinite. (For interpretation of the references to colour in this figure legend, the reader is referred to the web version of this article.)

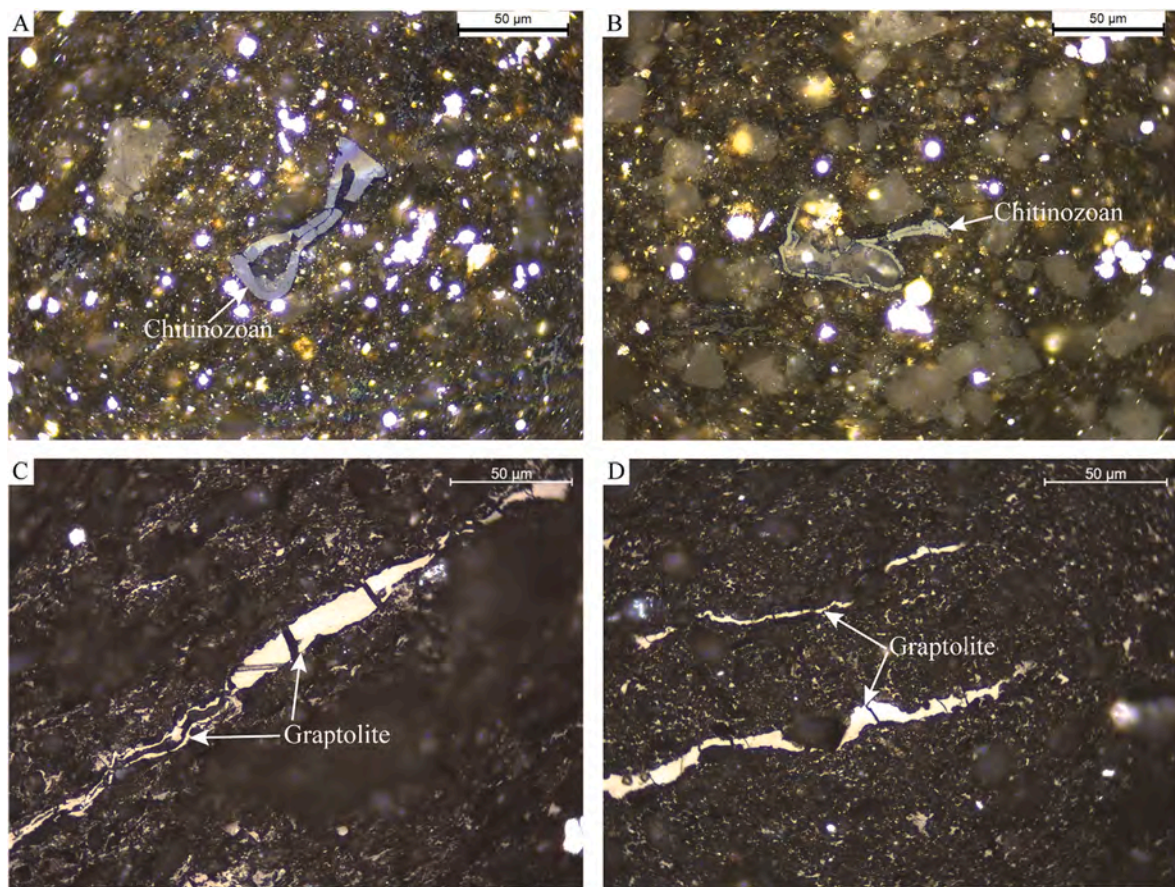


**Fig. 5.** Photomicrographs of chitinozoans (A, B) and graptolites (C, D) in reflected white light and oil immersion. (A) Core sample of the New Albany Shale from Gibson County, IN ( $R_o$  0.79%). (B) Core sample of the New Albany Shale from Daviess County, IN ( $R_o$  0.55%). (C, D) Outcrop sample of the Silurian Longmaxi Formation from Wuxi County, Chongqing, China ( $R_o$  equivalent 1.93%).

Vitrinite typically occurs as small particles dispersed in the mineral matrix of shales (Fig. 1). Because of its small size, vitrinite generally does not retain the cellular structure of vascular plants. In general, vitrinite is very rare in marine black shales. Mastalerz et al. (2018) suggested that for practical purposes, the term “vitrinite” could be used for all vitrinite group macerals in shales because recognizing individual macerals in the vitrinite group is difficult due to their scarcity and small particle size. In this study, “vitrinite” will be used to represent all vitrinite group macerals in black shales. In the case of shales rich in vitrinite, such as those in coal-bearing strata, maceral identification can be conducted based on the ICCP system 1994 (ICCP, 1998).

## 2.2. Inertinite

Inertinite in coals and shales is also derived from terrigenous OM (Taylor et al., 1998). It has almost no hydrocarbon generation potential and is typically classified as type IV kerogen. Originating as a result of fire or oxidation before deposition (Taylor et al., 1998), inertinite has very high reflectance even at early maturity. Similar to vitrinite, inertinite in shales occurs as dispersed particles in mineral matrix (Fig. 2). Cellular structures can be preserved in macerals fusinite and semi-fusinite. Because inertinite is also rare in black shales, “inertinite” will be used to represent all inertinite group macerals in black shales in this study. As with vitrinite, if inertinite content is high in shales, inertinite can be divided into different macerals based on the ICCP system 1994 (ICCP, 2001).

## 2.3. Liptinite

Liptinite group macerals are generally oil prone. They have high hydrocarbon generation potential and are typically classified as type I/II kerogen. Common liptinite macerals in black shales are alginite, amorphous organic matter (AOM; also named bituminite or amorphinitite), and liptodetrinite (Mastalerz et al., 2018). Alginite is derived from algae and occurs as elongated rods when viewed perpendicular to the bedding (Fig. 3A, B) and flattened disks on the bedding plane (Fig. 3C, D). Alginite shows strong greenish-yellow to yellow fluorescence under blue light irradiation at early maturity (Fig. 3B, D). AOM refers to structureless OM in black shales (Fig. 4A) and is derived from microbially degraded phytoplankton, zooplankton, and bacterial biomass (Kus et al., 2017; Liu et al., 2020a; Teng et al., 2021). It is the most common OM type in organic-rich shales. AOM can be further classified into multiple types based on fluorescence (Senftle et al., 1987), reflectance (Teng et al., 2021), and texture (Thompson and Demicki Jr, 1986; Kus et al., 2017). Because oil-prone AOM derived from algal material plays an important role in determining the hydrocarbon generation potential of black shales, it is the focus of this study. Liptodetrinite occurs as small discrete liptinite particles in the shale matrix and shows similar fluorescence to alginite (Fig. 4B). Liptinite macerals in black shales disappear after peak oil window ( $R_o$  0.8–1.0%) temperatures are reached because of transformation to oil and gas (Hackley and Cardott, 2016; Mastalerz et al., 2018; Liu et al., 2019a).

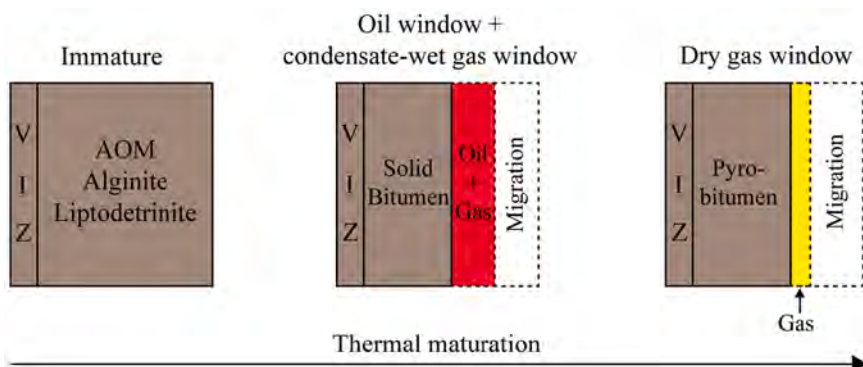


**Fig. 6.** Depiction of the evolution of macerals in black shales during thermal maturation. In the oil window and condensate-wet gas window, it is assumed that 50% of oil-prone organic matter was converted to oil and gas and that 50% of oil and gas migrated out of shale formations. The natural expulsion efficiency of shales varies significantly, depending on the petrophysical properties of shales and reservoir temperature and pressure conditions. V = vitrinite; I = inertinite; Z = zooclasts; AOM = amorphous organic matter.

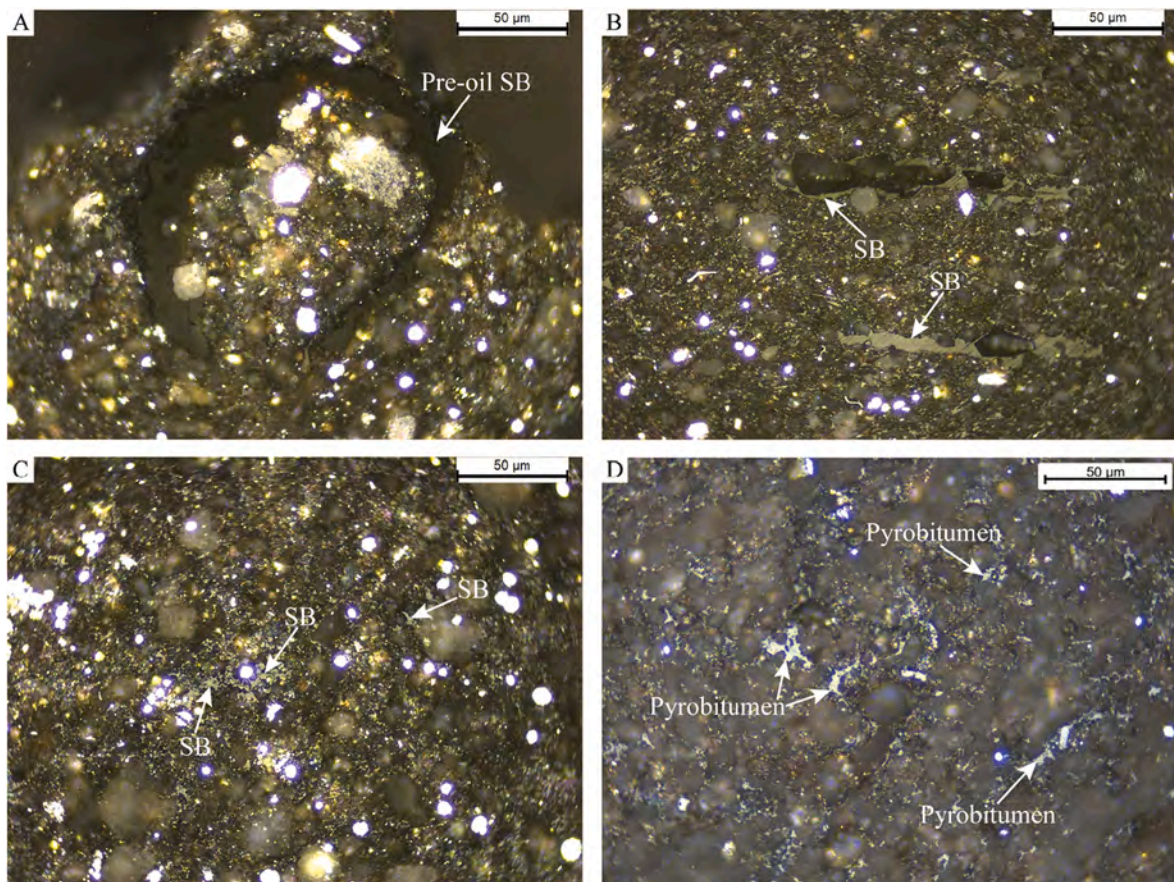


**Fig. 7.** Photomicrographs of solid bitumen (SB) and pyrobitumen in reflected white light and oil immersion. (A) Pre-oil SB transformed from alginite ( $R_o$  0.84%). The shape of precursor alginite can still be identified, suggesting that significant hydrocarbon generation has not started yet. Core sample of the New Albany Shale from Crittenden County, KY. (B) SB in the peak oil window ( $R_o$  0.98%). It is in the middle of hydrocarbon generation. Core sample of the New Albany Shale from Crittenden County, KY. (C) SB in the condensate-wet gas window ( $R_o$  1.18%). Outcrop sample of the New Albany Shale from Hicks Dome, IL. (D) Pyrobitumen in the dry gas window ( $R_o$  2.41%). Outcrop sample of the Marcellus Shale from Canastota, NY.

#### 2.4. Zooclasts

Zooclasts are fragments of zooplankton. Common zooplanktons in black shales include graptolites, chitinozoans, scolecodonts, and foram liners (Potter et al., 1998; Stasiuk et al., 2002; Mastalerz et al., 2018). They have low hydrocarbon generation potential and typically are gas prone. The reflectance of zooclasts can be used to assess the thermal maturity of host rocks in vitrinite-devoid shales, especially in pre-Devonian shales (e.g., Tricker et al., 1992; Petersen et al., 2013; Luo et al., 2017, 2020).

Zooclasts have partially preserved biological structures that impact

information about their origin. For example, zooclasts derived from chitinozoans can be identified based on their flask-shape organic-walled structure (Fig. 5A, B). Graptolites typically show parallel periderm (Fig. 5C, D). Generally, zooclasts are easy to distinguish from vitrinite and solid bitumen (SB) because of their distinct morphological attributes. However, when they occur as small particles without diagnostic morphological traits, it can be difficult to identify them with confidence; they could be mistaken for vitrinite (Petersen et al., 2013; Liu et al., 2020b).

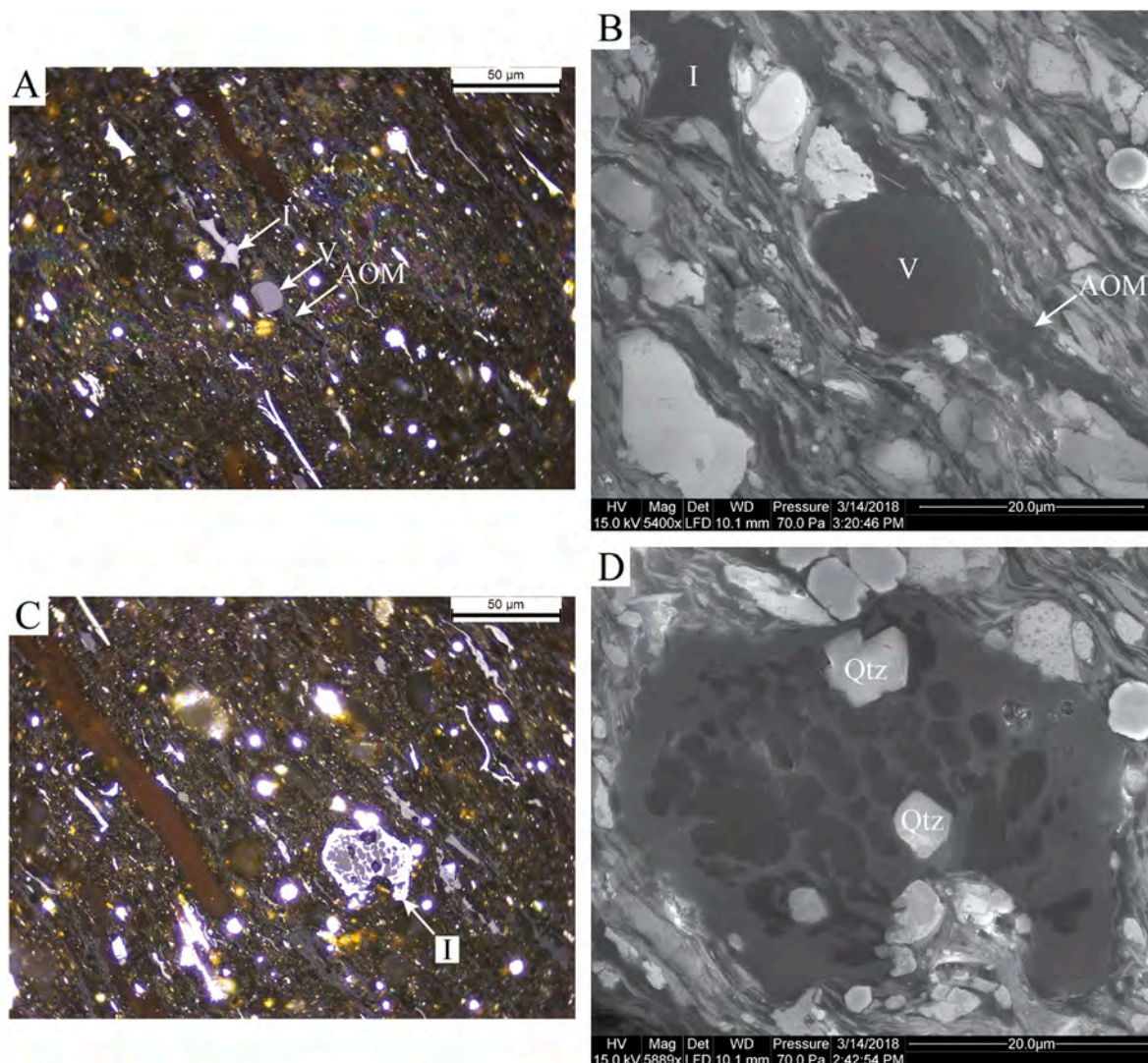


**Fig. 8.** Photomicrographs of vitrinite and inertinite in reflected white light and oil immersion (A, C) and under SEM (B, D, secondary electron mode). Vitrinite and inertinite in panels B and D are the same particles in panels A and C, respectively, but under different magnification. Inertinite in panel D has cellular pores, some of which are filled with diagenetic quartz. Core sample of the New Albany Shale from Daviess County, IN ( $R_o$  0.55%). V = vitrinite; I = inertinite; Qtz = quartz.

## 2.5. Secondary organic matter

Secondary OM refers to OM generated during thermal maturation of primary oil-prone OM and consists of SB, pyrobitumen, and oil (Potter et al., 1998; Stasiuk et al., 2002; Mastalerz et al., 2018). SB includes pre-oil and post-oil SB (Mastalerz et al., 2018). SB becomes the dominant OM after peak oil window temperatures are reached, because oil-prone macerals are transformed to hydrocarbons and SB (Fig. 6; Cardott et al., 2015; Hackley and Cardott, 2016; Mastalerz et al., 2018; Liu et al., 2019a; Sanei, 2020). Because the transformation of oil-prone macerals occurs across a continuum, pre-oil SB, post-oil SB, and SB in the middle of oil generation can co-exist in the same sample, especially at early maturity and in the peak oil window. SB transforms to pyrobitumen through secondary cracking in the dry gas window (Fig. 6). Mastalerz et al. (2018) proposed that a SB reflectance of 1.5% should be used as the boundary value for SB and pyrobitumen and 1.3% in the case of sulfur-rich kerogen. The chemical and physical properties and origin of SB and pyrobitumen were comprehensively reviewed in Mastalerz et al. (2018) and Sanei (2020). Because SB reflectance and  $R_o$  are positively correlated, SB reflectance can be used to estimate the thermal maturity of shales when vitrinite is absent (Jacob, 1989; Landis and Castaño, 1995; Schoenherr et al., 2007; Hackley and Cardott, 2016; Mastalerz et al.,

2018; Liu et al., 2019a; Schmidt et al., 2019). However, SB could be mistaken for vitrinite and result in underestimating the thermal maturity of black shales at low maturity ( $R_o \leq 1.0\%$ ; Hackley and Lewan, 2018).

Solid bitumen and pyrobitumen were once high-viscosity liquids and thus fill void spaces between and within mineral grains. Because of that, they typically show embayment texture when in contact mineral grains (Fig. 7). SB and pyrobitumen can be distinguished from vitrinite and zooclasts based on their void-filling or embayment textures, and from AOM on the basis of their homogeneous surface in addition to other identifying textures (Hackley et al., 2018).

It is important to note that SB and bitumen are defined differently. SB is organic petrographically defined and refers to solid secondary OM identified under an optical microscope (Mastalerz et al., 2018), whereas bitumen is organic geochemically defined and refers to OM that can be extracted with organic solvents such as chloroform (Durand, 1980). SB in the oil window may be partially soluble in organic solvents (Hackley and Cardott, 2016), and its solubility decreases with increasing maturity. Pyrobitumen is largely insoluble in organic solvents (Mastalerz et al., 2018). The term kerogen, in contrast to bitumen, refers to solid OM that cannot be extracted with organic solvents (Durand, 1980). Thus, kerogen corresponds to the insoluble fraction of SB in the oil

**Table 1**

Simplified petrographic classification of dispersed organic matter (DOM) in black shales (modified from Mastalerz et al. (2018) and references therein), comments on macerals, and petrographic characteristics of macerals under the scanning electron microscope (SEM).

Maceral Group	Maceral	Comments	SEM Petrography
Vitrinite		“vitrinite” is used to represent all vitrinite group macerals because of their scarcity and small size in shales.	Dispersed OM particles in the mineral matrix.
Inertinite		“inertinite” is used to represent all inertinite group macerals because of their scarcity and small size in shales.	Dispersed OM particles in the mineral matrix. Some inertinite has cellular structure, which can be used as an identifying feature. Inertinite can be difficult to distinguish from vitrinite if cellular structure is not present.
Liptinite	Alginite	Well-preserved algal cysts. <i>Boryococcus</i> , <i>Tasmanites</i> , and <i>Leiosphaeridia</i> are common algae preserved in shales.	Alginite can be easily identified based on their distinct shapes of algal bodies. Note that alginite occurs as elongated rods perpendicular to the bedding and flattened disks parallel to the bedding. In lacustrine shales, alginite and sporinite can look similar. Alginite generally does not exist above $R_o$ 1.0%. AOM occurs as structureless OM streaks and has clay-sized mineral inclusions. AOM generally does not exist above $R_o$ 1.0%.
Zooclasts	Amorphous organic matter (oil-prone AOM derived from algal material)	Also named amorphinitite/ bituminite	Dispersed OM particles in the mineral matrix. Zooclasts can be identified based on their morphology if some diagnostic characteristics are preserved. Otherwise, they are difficult to distinguish from vitrinite and inertinite.
Secondary organic matter	Solid bitumen	Dominant OM after peak oil window ( $R_o$ 0.8–1.0%) in shales with type I/II kerogen.	SB can be identified based on void-filling or embayment textures against minerals, especially euhedral crystals. SB can be difficult to distinguish from AOM at early maturity.
	Pyrobitumen	Dominant OM in the dry gas window in shales with type I/II kerogen. SB.	Pyrobitumen has similar occurrence to SB.

**Table 1 (continued)**

Maceral Group	Maceral	Comments	SEM Petrography
	Oil	reflectance 1.50% (1.30 for S-rich kerogen) is used as the thermal maturity boundary between SB and pyrobitumen.	Oil droplets of various shapes. The morphology of oil droplets changes during electron scanning.

OM = organic matter; AOM = amorphous organic matter; SB = solid bitumen.

window and condensate-wet gas window, and to pyrobitumen in the dry gas window.

### 3. SEM petrography of dispersed organic matter

#### 3.1. Vitrinite and inertinite

Because both vitrinite and inertinite are particulate OM, they occur as discrete OM particles in the shale matrix (Fig. 8; Table 1) and can be difficult to distinguish from each other under the SEM. Some inertinite has angular outlines and/or cellular structures derived from cell lumens of vascular plants, which can be used as identifying features. The cellular structures are generally filled with early diagenetic minerals such as quartz and pyrite (Liu et al., 2017).

#### 3.2. Liptinite

Alginite can be identified under the SEM on the basis of the distinct shape of algal bodies (Fig. 9; Table 1). AOM has a heterogeneous surface and shows admixed nature with clay-sized mineral grains and other particles (Fig. 10). It can be difficult to distinguish AOM from SB at early maturity (Hackley et al., 2018), but SB typically has a homogeneous surface and shows void-filling and embayment textures (Fig. 7).

#### 3.3. Zooclasts

Similar to alginite, zooclasts can be identified under the SEM based on the distinct biological structure of the zooplankton precursor (Fig. 11; Table 1). However, if no diagnostic morphology accompanies zooclasts, they can be difficult to distinguish from vitrinite and inertinite under the SEM, as well as with an optical microscope (Petersen et al., 2013; Liu et al., 2020b).

#### 3.4. Secondary organic matter

Solid bitumen and pyrobitumen can be identified under the SEM based on their void-filling or embayment textures (Fig. 12; Table 1). OM that fills fossil cavities such as foraminifera tests is by definition secondary in nature (Loucks and Reed, 2014; Milliken et al., 2014; Schieber et al., 2016; Reed et al., 2020). The morphology of SB and pyrobitumen is constrained by the shape of the pores they infill. Although pore systems and their SB infills are three dimensional and continuous, when sectioned the SB can/will appear as isolated particles and become difficult to distinguish from other particulate OM such as vitrinite, inertinite, and small zooclast particles under the SEM.

Under an optical microscope, the presence of oil may be indicated by iridescent films on mineral grains when the sample is examined without the help of immersion oil. When immersion oil is used, the oil from the sample will mix with the immersion oil and will no longer be visible in reflected white light, but can be detected under fluorescence light

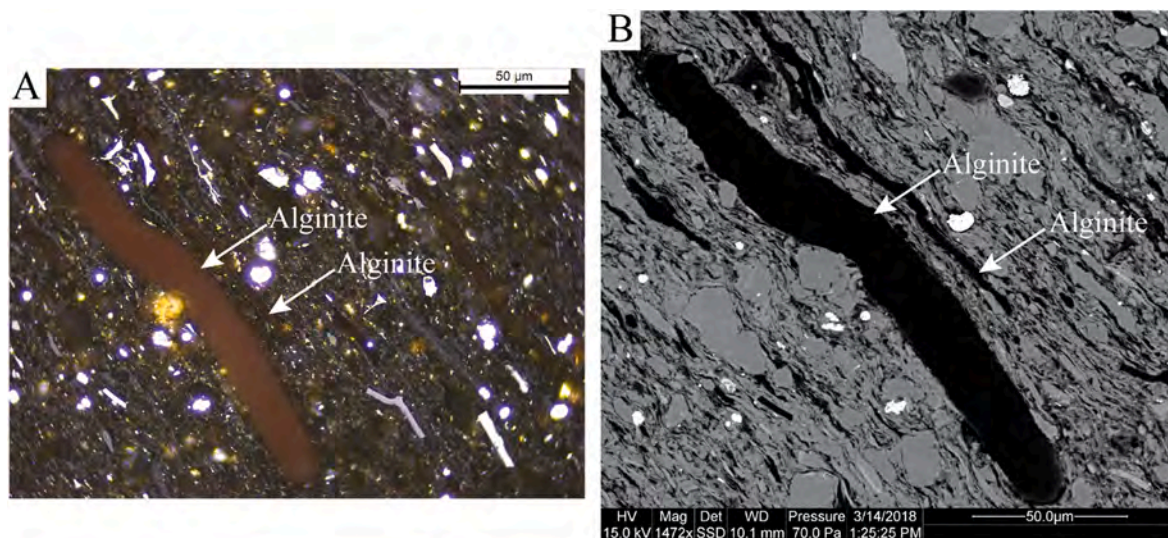


**Fig. 9.** Photomicrographs of alginite derived from *Tasmanites* cysts in reflected white light and oil immersion (A) and under SEM (B, backscattered electron mode). Core sample of the New Albany Shale from Daviess County, IN ( $R_o$  0.55%).

(Ardakani et al., 2017). Under the SEM oil may be visible as variably shaped droplets (O'Brien et al., 1996; Canter et al., 2016) that change shape and size as they get heated and vaporized by the electron beam (Fig. 13).

### 3.5. Strategies for distinguishing dispersed organic matter under SEM

It is a challenging task to confidently identify OM types with the SEM alone because all OM appears black under the SEM in backscattered electron mode due to their low density (Camp, 2016; Kwiecińska et al., 2019; Valentine and Hackley, 2019). Organic petrographic distinguishing criteria under an optical microscope such as colour, reflectance, and fluorescence cannot be used in SEM petrography. Camp (2016) proposed to classify DOM in shales into three main types under the SEM: 1) structured, 2) amorphous, and 3) void-filling. However, although this morphology-based classification is convenient to describe DOM under the SEM, the information on the origin of DOM is missing. Loucks and Reed (2014) distinguished depositional OM (kerogen) and migrated OM (SB and pyrobitumen) in mudrocks under the SEM. Likewise, Bernard et al. (2012) identified kerogen, bitumen, and pyrobitumen in the Lower Toarcian Posidonia Shale using scanning transmission X-ray microscopy. Milliken et al. (2014) classified OM in OM-rich mudrocks into detrital OM, secondary OM, and OM of uncertain origin under the SEM. However, the term “kerogen”, “depositional OM”, or “detrital OM” is too broad and ignores the heterogeneity of OM in black shales. The DOM classification used by organic petrographers still remains the best method in describing DOM in black shales under the SEM (Table 1). Cardott and Curtis (2018) differentiated maceral groups and some macerals in coals by SEM based on gray scale, occurrence, shape, and structure in backscattered electron mode at low magnification ( $\leq 2500\times$ ). They did suggest that maceral identification in shales is more difficult because of the lack of subtle contrast of adjacent macerals.

Correlative microscopy is a powerful approach to distinguish DOM types under the SEM, relying on organic petrographic identification of DOM before proceeding to high-resolution imaging under the SEM (Hackley et al., 2017; Liu et al., 2017, 2020a; Valentine and Hackley, 2019; Hackley et al., 2021; Wei et al., 2021). When conducting correlative microscopy, macerals are first identified under an optical microscope with reflected white light and oil immersion. The surfaces of petrographic pellets are subsequently cleaned to remove immersion oil, and then the pellets are cut for SEM sample preparation. The same surfaces as observed under reflected-light microscopy are Ar ion-milled

for SEM observations, and the same fields of view need to be located under the SEM (Fig. 14). Microfractures, pyrite framboids, or fossils can be used as markers for easier identification. Alternatively, OM can be first examined on ion-milled surfaces under the SEM, and then samples can be moved to the reflected-light microscope for maceral identification. In this case, additional sample preparation is unnecessary. However, ion-milled samples may have increased surface flatness and resulting higher reflectance compared to mechanically polished samples (Mastalerz and Schieber, 2017; Valentine et al., 2019), thus they may be not suitable for reflectance measurements and maturity assessment. Hackley et al. (2017) differentiated fluorescent AOM and nonfluorescent SB using integrated correlative microscopy that combines fluorescence microscopy and SEM. Liu et al. (2017) identified AOM, alginite, vitrinite, inertinite, and solid bitumen in the New Albany Shale using correlative microscopy and studied maceral control on organic pores development. Valentine and Hackley (2019) identified various macerals in multiple North American shale petroleum systems via correlative light and electron microscopy and suggested that OM type can be easily misidentified when viewed by SEM alone.

Oil-prone macerals such as AOM (those derived from algal material) and alginite are generally not present after the peak oil window ( $R_o$  0.8–1.0%) because of their transformation to hydrocarbons and SB (Fig. 15; Hackley and Cardott, 2016; Mastalerz et al., 2018; Liu et al., 2019a; Sanei, 2020). Therefore, OM in high-maturity shales is dominated by SB or pyrobitumen if OM in those shales was dominated by oil-prone macerals during the immature stage.

Because terrigenous OM (e.g., vitrinite and inertinite) and zooclasts do not transform to hydrocarbons and solid bitumen during thermal maturation due to their low hydrocarbon generation potential, they can exist at any stage of thermal maturation. If terrigenous OM dominates OM composition in immature shales such as some lacustrine shales with high terrigenous OM input, vitrinite and inertinite will be the dominant OM throughout the maturation process even after shales enter the dry gas window. An extreme case is coal where vitrinite and inertinite are still present at higher coal rank. Because both terrigenous OM and zooclasts occur as dispersed OM particles, it can be difficult to distinguish them from each other under the SEM. Some features of specific macerals can aid the identification such as the cellular structure of inertinite (Figs. 2, 8C, D) and the flask-shape structure of chitinozoans (Fig. 5A, B).

Differentiating OM under the SEM is an achievable task if there is a good understanding of the studied shales, especially knowledge about

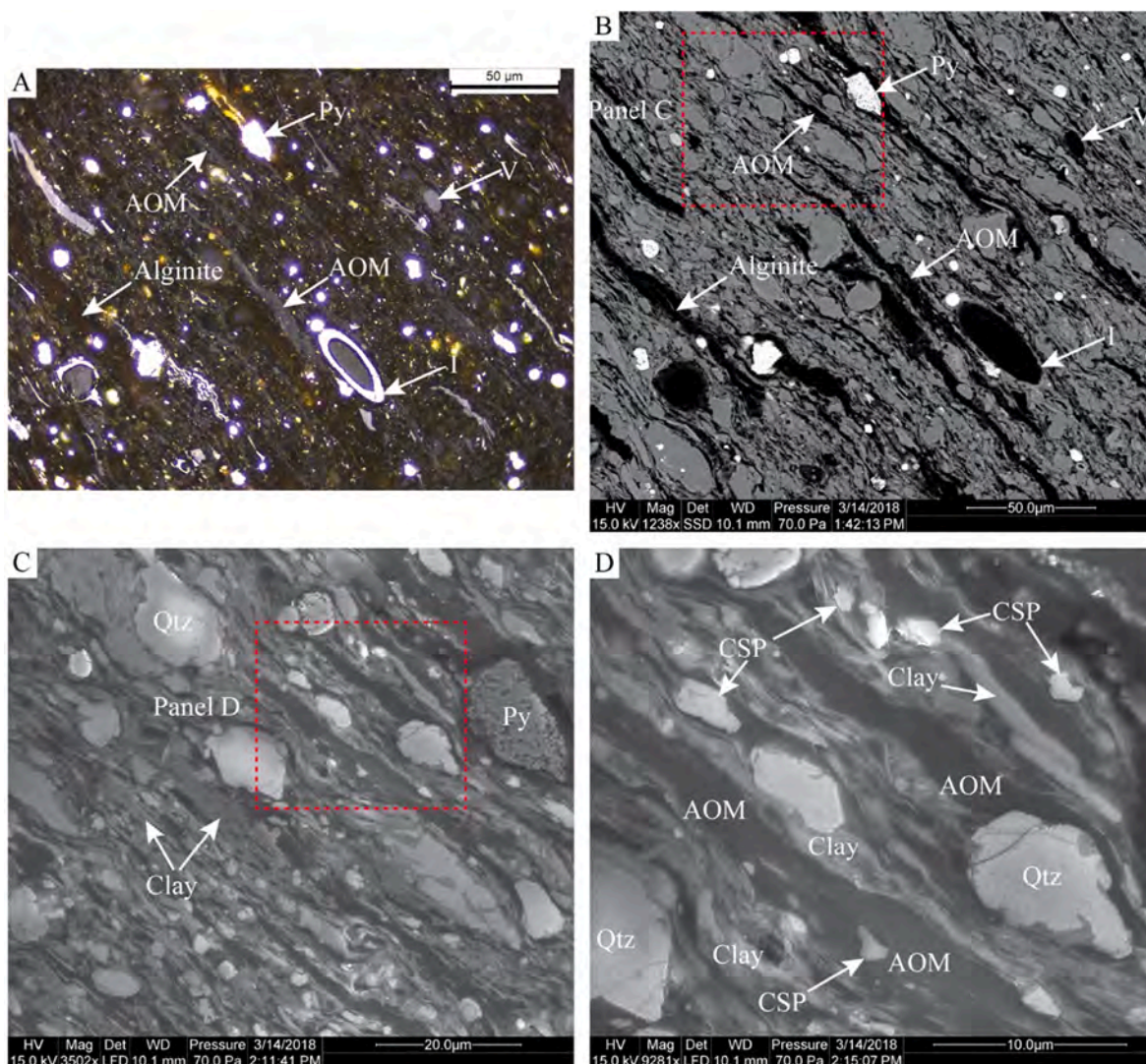


**Fig. 10.** Photomicrographs of amorphous organic matter (AOM) in reflected white light and oil immersion (A) and under SEM (B, backscattered electron mode; C, D, secondary electron mode). Panel A and B show the same field of view. Panels C and D are the close-up views of the red dashed areas in panels B and C, respectively. Note that AOM is mixed with clay minerals and clay-sized particles, which gives AOM a heterogeneous appearance. Clay-sized particles in panel D are most likely diagenetic quartz. Core sample of the New Albany Shale from Daviess County, IN ( $R_o = 0.55\%$ ). AOM = amorphous organic matter; V = vitrinite; I = inertinite; Py = pyrite; Qtz = quartz; CSP = clay-sized particle. (For interpretation of the references to colour in this figure legend, the reader is referred to the web version of this article.)

the OM composition of immature or early mature samples (if low-maturity samples are available) and the thermal maturity of the specific samples being examined. A dataset of OM composition for a specific shale formation across a maturation gradient greatly assists in the identification and differentiation of OM under the SEM. For example, Mastalerz et al. (2016b) published an atlas of photomicrographs of OM in the Upper Devonian New Albany Shale of the Illinois Basin at different stages of thermal maturation ( $R_o < 0.5$  to  $1.42\%$ ). OM in the immature and early mature New Albany Shale is dominated by oil-prone macerals such as AOM and alginite derived from *Tasmanites* cysts (Liu et al., 2017, 2019a, 2019b; Mastalerz et al., 2012, 2013, 2016b). Terrigenous OM including vitrinite and inertinite is generally less than 5% (Liu et al., 2019b, 2020a). It also contains minor amounts of zooclasts derived from chitinozoans (Liu et al., 2020b). If a New Albany Shale sample with a thermal maturity of  $R_o = 1.42\%$  is examined under the SEM, more than 95% of the OM would be SB. Based on void-filling and embayment textures, the OM in Fig. 16 can confidently be identified as SB.

#### 4. Development and preservation of organic matter-hosted pores

Organic matter-hosted pores in black shales have been extensively studied since Loucks et al. (2009) reported organic pores in the Mississippian Barnett Shale of the Fort Worth Basin. OM-hosted pores contribute significantly to the gas content and methane adsorption capacity of black shales (Ross and Bustin, 2009; Hao et al., 2013; Qiu et al., 2020a) due to their microporous structure and high specific surface area (SSA) (Bousige et al., 2016; Liu et al., 2021).

Organic matter-hosted pores in black shales include primary and secondary organic pores (Löhr et al., 2015; Liu et al., 2017; Cardott and Curtis, 2018; Katz and Arango, 2018; Dong et al., 2019; Wu et al., 2020). Primary organic pores are hosted by primary macerals such as inertinite and are derived from the biological structure of original OM (Figs. 2, 8C, D). In comparison, secondary organic pores are hosted by solid bitumen or pyrobitumen and are related to hydrocarbon generation and expulsion from oil-prone OM. The development and preservation of secondary OM-hosted pores are controlled by thermal maturity, OM type and

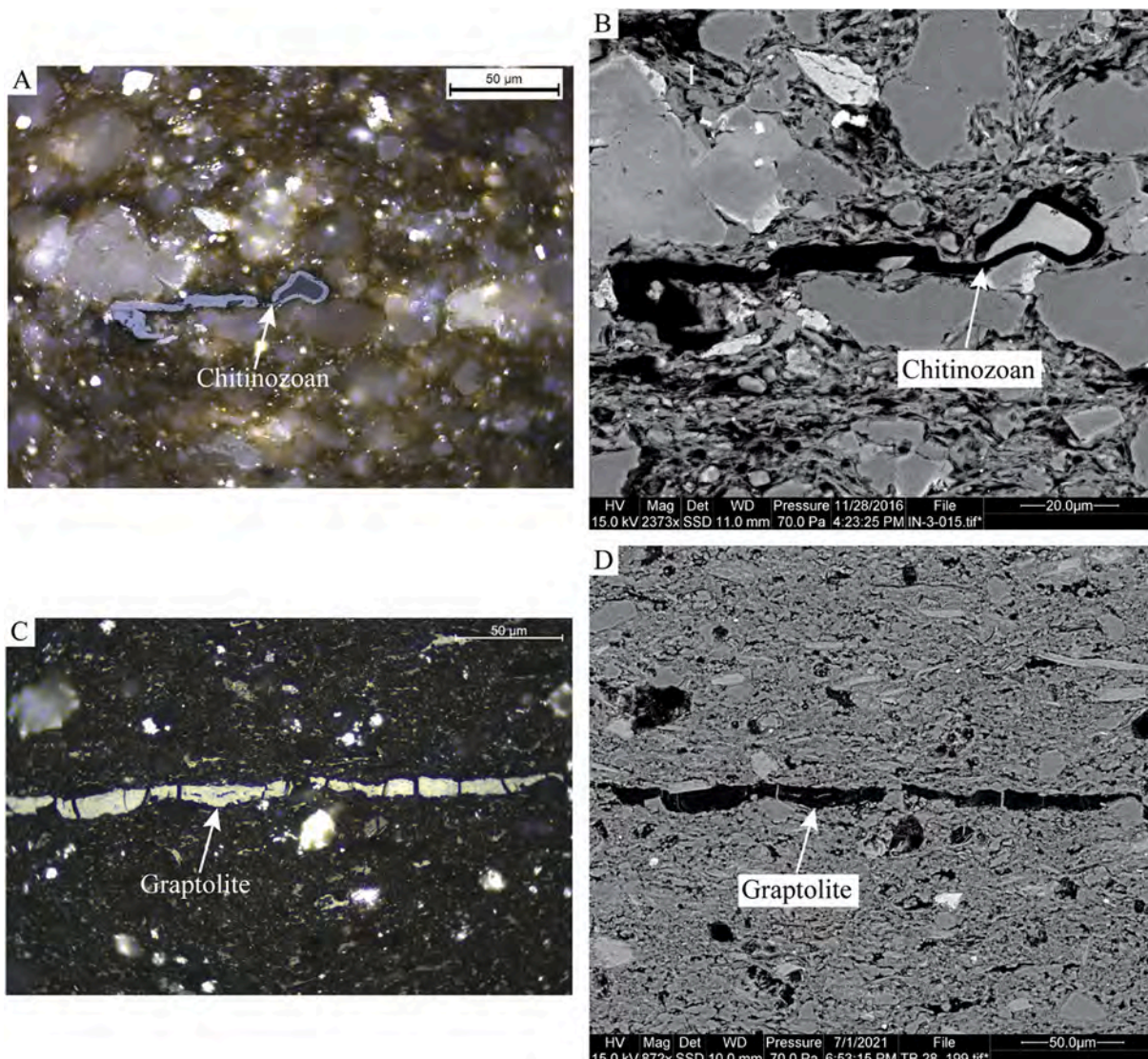


**Fig. 11.** Photomicrographs of zooclasts in reflected white light and oil immersion (A, C) and under SEM (B, D, backscattered electron mode). (A, B) Chitinozoan. Core sample of the New Albany Shale from Daviess County, IN ( $R_o$  0.55%). (C, D) Graptolite. Outcrop sample of the Silurian Longmaxi Formation from Wuxi County, Chongqing, China ( $R_o$  equivalent 1.93%).

content (e.g., Liu et al., 2017; İnan et al., 2018; Katz and Arango, 2018; Mastalerz et al., 2018). The evolution of OM-hosted pores was comprehensively reviewed in Katz and Arango (2018).

#### 4.1. Control of organic matter type

Oil-prone macerals transform to hydrocarbons and SB or pyrobitumen during thermal maturation (Fig. 15; Hackley and Cardott, 2016; Mastalerz et al., 2018; Liu et al., 2019a; Sanei, 2020). Secondary OM-hosted pores develop in SB or pyrobitumen after oil and gas expulsion (Liu et al., 2017; İnan et al., 2018; Katz and Arango, 2018; Mastalerz et al., 2018; Camp, 2019). Because SB and pyrobitumen were once liquid, they can form an interconnected network of porous OM (Liu et al., 2019a), forming an organic pore network and connecting pores associated with minerals. In contrast, terrigenous OM including vitrinite and inertinite does not show significant changes in morphology during thermal maturation due to its low hydrocarbon generation potential (Liu et al., 2019a). It is noteworthy though that vitrinite in coals does develop secondary pores due to generation and expulsion of gaseous hydrocarbons (Zhang et al., 2003). The absence of secondary pores in dispersed vitrinite in shales could be because of its low potential for hydrocarbon

generation (Liu et al., 2017). Although inertinite does not develop secondary pores, it can host primary cellular pores (Figs. 2, 8C, D). The size of cellular pores is generally in the range of hundreds of nm to tens of  $\mu\text{m}$ . Cellular pores are typically filled with early diagenetic minerals such as quartz and pyrite and make very limited contribution to the pore system of shales (Liu et al., 2017). Zooclasts such as graptolite and chitinozoan have similar or lower hydrocarbon generation potential compared to vitrinite (Bertrand and Héroux, 1987; Bustin et al., 1989; Goodarzi and Norford, 1989; Bertrand, 1990; Petersen et al., 2013; Reyes et al., 2018; Zheng et al., 2021) and have been reported to not develop secondary pores during thermal maturation when examined under the SEM (Ardakani et al., 2018; Yang et al., 2020). However, other studies have found organic pores within graptolites (e.g., Luo et al., 2016; Ma et al., 2016; Qiu et al., 2018; Gong et al., 2020; Tenger et al., 2021). It is still not clear if these pores are secondary pores generated during hydrocarbon generation and expulsion or primary pores derived from the biological structure of graptolites, or if these pores just occur in solid bitumen that filled and/or coated graptolites.

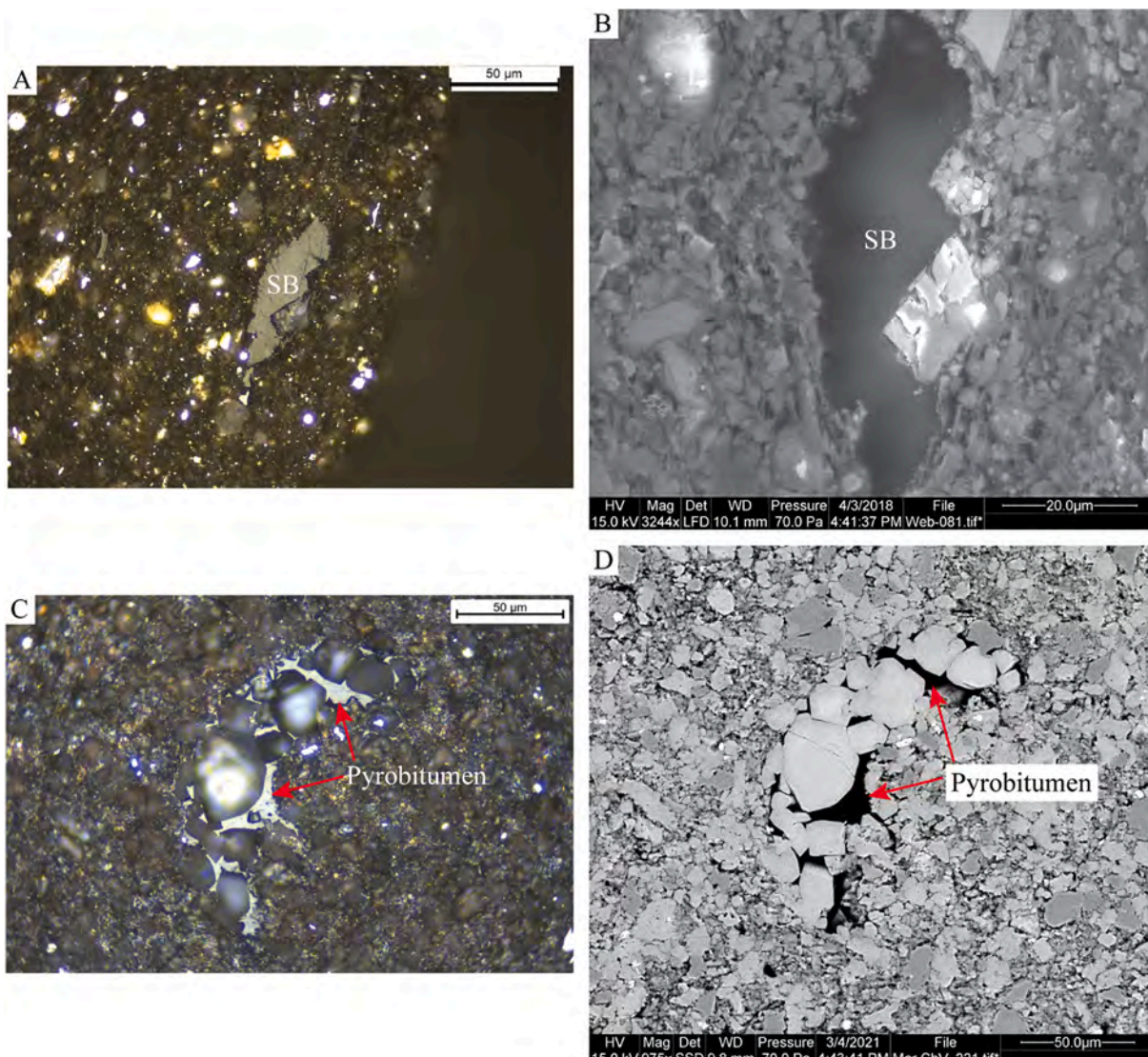


**Fig. 12.** Photomicrographs of solid bitumen (SB) and pyrobitumen in reflected white light and oil immersion (A, C) and under SEM (secondary electron mode; D, backscattered electron mode). Note the embayment texture of SB and pyrobitumen against minerals. (A, B) Core sample of the New Albany Shale from Webster County, KY ( $R_o$  0.80%). (C, D) Outcrop sample of the Marcellus Shale from Canastota, NY ( $R_o$  2.41%).

#### 4.2. Control of thermal maturity

The development of secondary OM-hosted pores has been explained to be the result of hydrocarbon generation and expulsion (e.g., Loucks et al., 2009, 2012; Schieber, 2010; Bernard et al., 2012; Curtis et al., 2012; Liu et al., 2017; İnan et al., 2018; Katz and Arango, 2018; Matalerz et al., 2018). Secondary OM-hosted pores do not exist in immature shales and start to form at the onset of hydrocarbon generation. The lowest maturity at which OM-hosted pores might form has been suggested to be  $R_o$  0.6% (Loucks et al., 2012). OM-hosted pores are more abundant in the gas window than in the oil window because 1) gas generation and expulsion in the gas window are more favorable for the formation of OM-hosted pores, and 2) bitumen and oil migration in the oil window can fill newly formed OM-hosted pores and make them less visible under the SEM.

#### 4.3. Control of organic matter content

As with mineral matrix-associated pores, OM-hosted pores experience formation, preservation, and destruction during burial. Fundamentally, the formation of OM-hosted pores is controlled by the

chemical and physical properties of the OM and reservoir temperature and pressure conditions. OM content, generally characterized by total organic carbon (TOC) content, does not affect the formation process of organic pores, but it can influence their preservation (Fishman et al., 2012; Milliken et al., 2013; İnan et al., 2018; Katz and Arango, 2018). For example, Milliken et al. (2013) reported that Marcellus Shale samples with higher TOC contents show lower SEM-visible organic porosity because of greater OM connectivity and elevated compaction. However, compaction will mostly affect the SEM-visible macropores ( $> 50$  nm) and large mesopores (2–50 nm; Rouquerol et al., 1994) and will have very limited influence on micropores ( $< 2$  nm; Rouquerol et al., 1994) and small mesopores (Ma et al., 2020), because once OM is compacted and squeezed into interparticle pores between mineral grains, it will be protected by rigid mineral grains from further compression (Knapp et al., 2020). In addition, bitumen transformed from oil-prone OM migrates into mineral matrix-associated pores and thus becomes less prone to further compaction.

Mineralogical composition also plays an important role in preserving OM-hosted pores. Hard quartz-rich (especially biogenic quartz) and carbonate-rich shales can better preserve OM-hosted pores than ductile clay-rich shales because rigid quartz and carbonate can protect organic

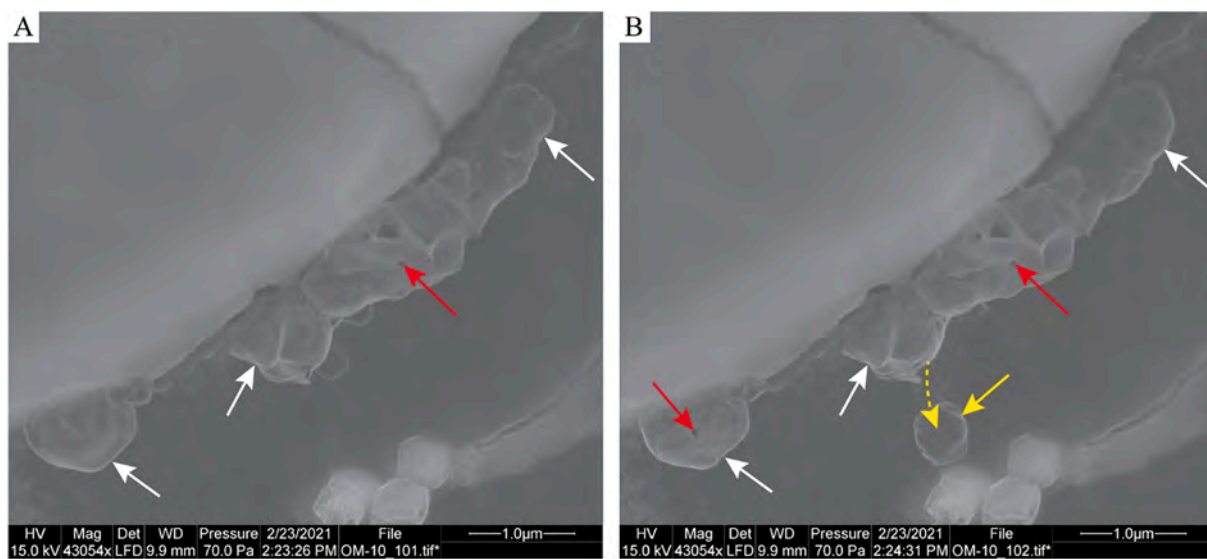


**Fig. 13.** SEM images (secondary electron mode) of oil droplets (white arrows). Image B was taken in the same field of view as image A after 1 min of scanning. Black holes marked by red arrows were artificially made by heating with the electron beam. After 1 min of scanning, an oil droplet (yellow arrow) moved along the yellow dashed arrow. Core sample of the New Albany Shale from Daviess County, IN ( $R_o$  0.55%). (For interpretation of the references to colour in this figure legend, the reader is referred to the web version of this article.)

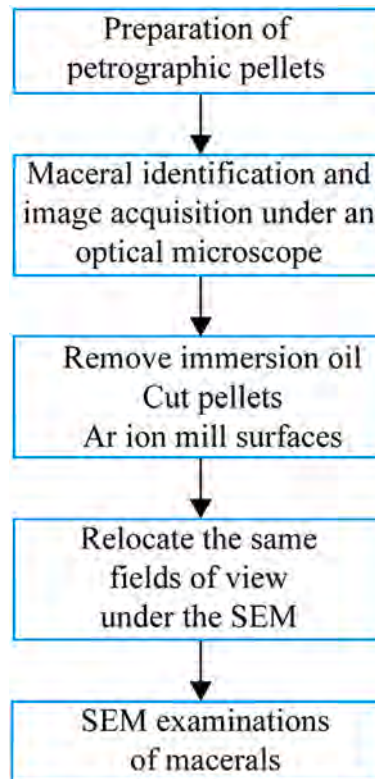


**Fig. 14.** Work flow of correlative light and electron microscopy for organic matter type identification under the SEM.

pores from mechanical compaction (Fishman et al., 2012; İnan et al., 2018; Dong and Harris, 2020; Knapp et al., 2020; Qiu et al., 2020b, 2022). For example, Fishman et al. (2012) suggested that the quartz-rich Barnett Shale and carbonate-rich Eagle Ford Shale can better preserve delicate organic pores than the clay-rich Kimmeridge Shale because the former two have a rigid interconnected framework composed of diagenetic quartz and carbonate, respectively.

## 5. Evolution of organic matter-hosted pores during thermal maturation

The size of secondary OM-hosted pores is generally  $<1000$  nm (Figs. 17, 18) and can be as small as  $<1$  nm (Loucks et al., 2009, 2012; Wang et al., 2009; Schieber, 2010; Strapoć et al., 2010; Mastalerz et al., 2013; Bousige et al., 2016). OM-hosted pores are generally observed on

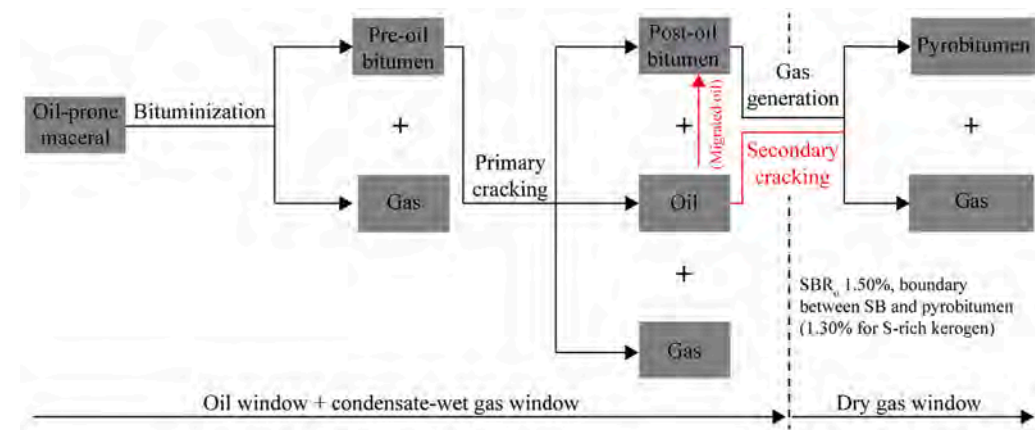


**Fig. 15.** Diagram illustrating the evolutionary pathway of oil-prone macerals during thermal maturation. Migrated oil refers to oil that has migrated into conventional reservoirs. Compiled and modified after [Jarvie et al. \(2007\)](#); [Bernard and Horsfield \(2014\)](#); [Camp \(2016\)](#); [Mastalerz et al. \(2018\)](#).

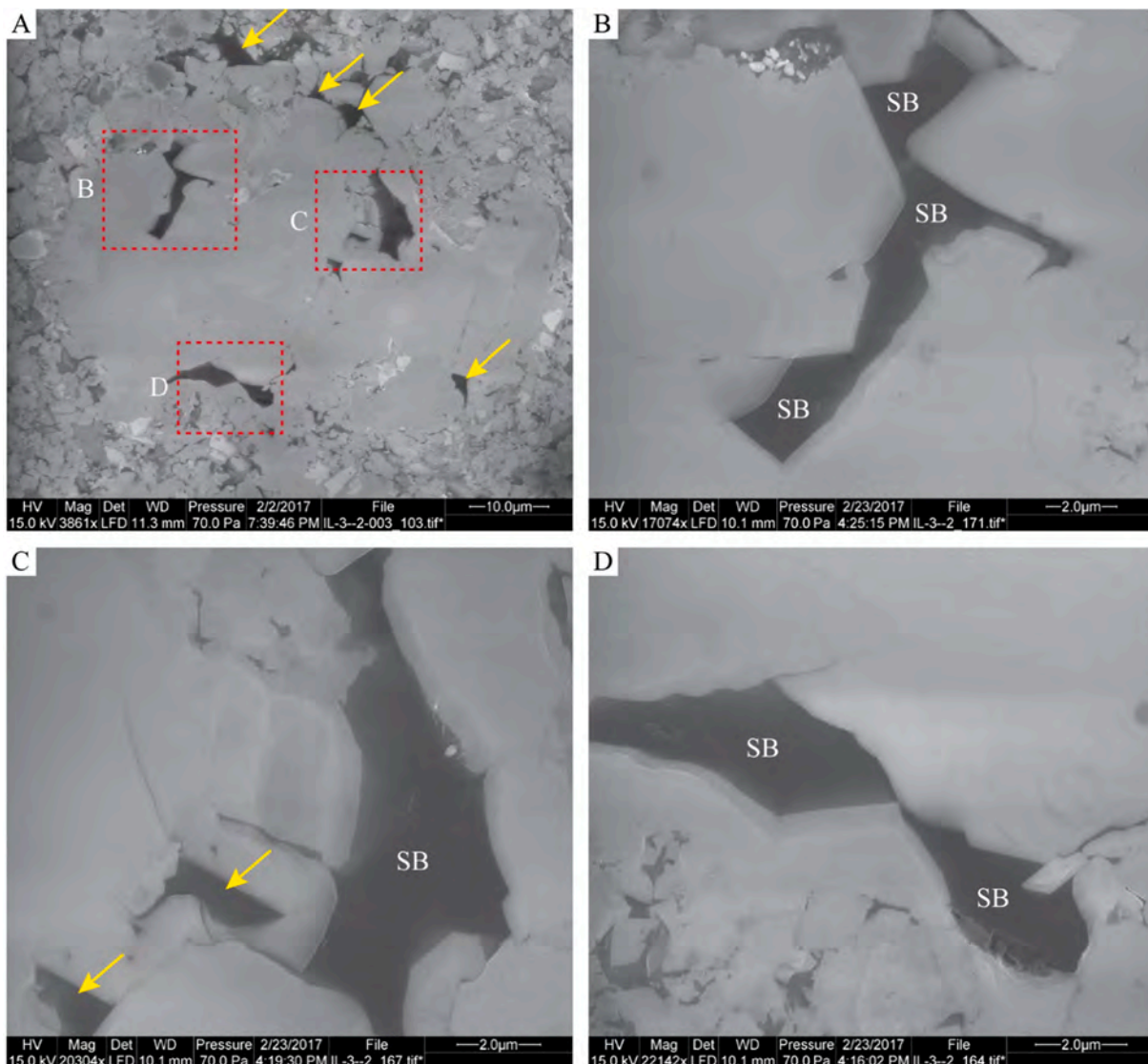


**Fig. 16.** SEM (secondary electron mode) images of organic matter (OM) in the New Albany Shale ( $R_o$  1.42%). OM is identified as solid bitumen (SB) based on its void-filling texture and embayment against euhedral crystals as well as its level of thermal maturity. Small SB is also indicated by yellow arrows. Outcrop sample of the New Albany Shale from Hicks Dome, IL. (For interpretation of the references to colour in this figure legend, the reader is referred to the web version of this article.)

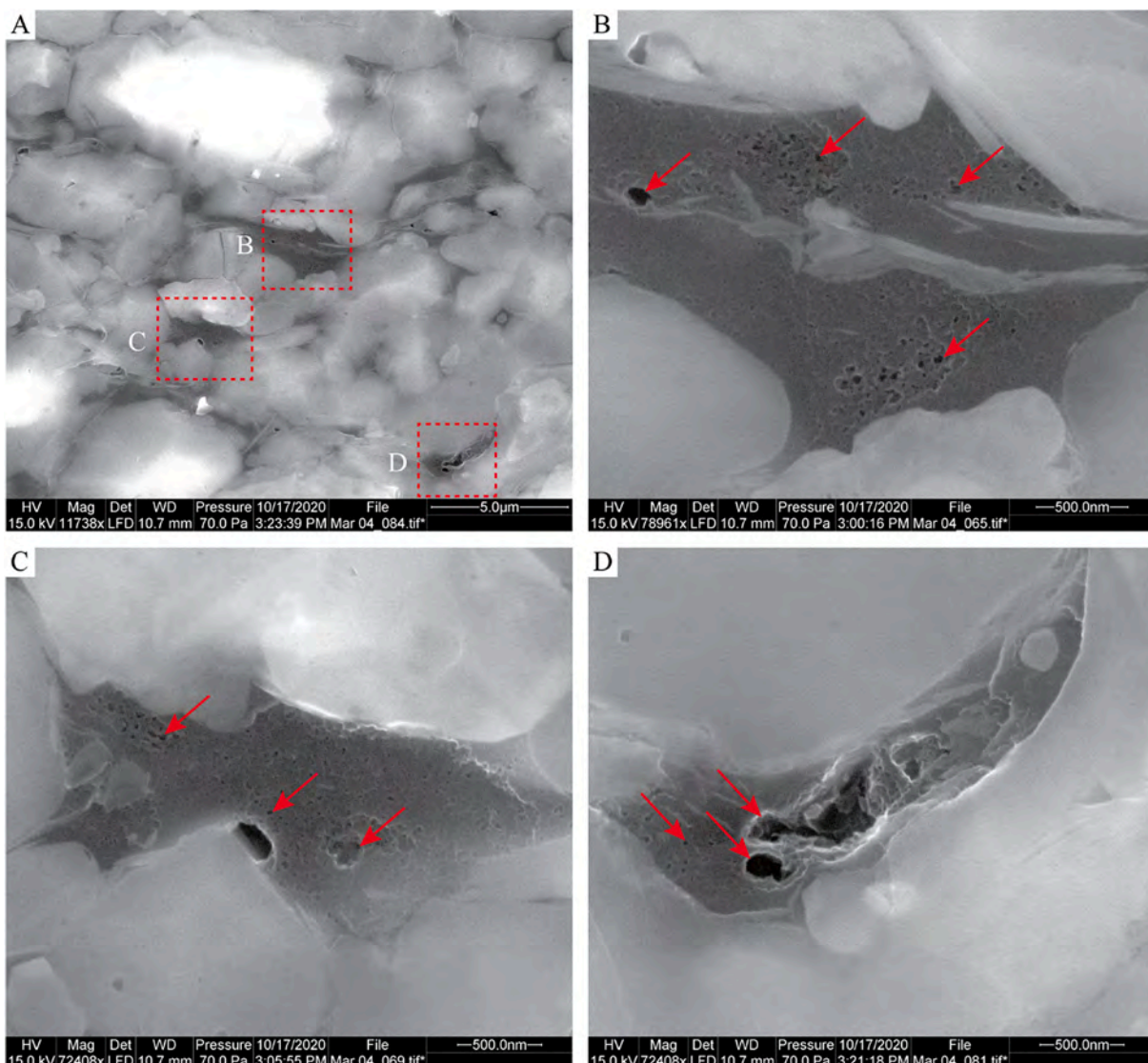


**Fig. 17.** SEM (secondary electron mode) images of organic matter (OM)-hosted pores (red arrows) in the Marcellus Shale ( $R_o$  2.41%). OM in the images is pyrobitumen based on thermal maturity and void-filling and embayment textures. Outcrop sample of the Marcellus Shale from Canastota, New York. (For interpretation of the references to colour in this figure legend, the reader is referred to the web version of this article.)

Ar ion-milled surfaces under the SEM. However, due to resolution limitations, SEM imaging is not able to detect pores smaller than 5 nm (Mastalerz et al., 2018). Low-pressure N<sub>2</sub> and CO<sub>2</sub> adsorption analyses show that OM has abundant pores smaller than 5 nm, even at early maturity. These small pores are void spaces within the macromolecular structure of OM (Bousige et al., 2016) and contribute significantly to the SSA of shales.

The Brunauer-Emmett-Teller (BET) SSA of OM isolated from black shales increases with increasing thermal maturity and reaches a maximum (~ 300 m<sup>2</sup>/g) at  $R_o$  2.5–3.0% (Fig. 19A). When  $R_o$  exceeds 3.0%, the BET SSA of OM starts to decrease with further increase of thermal maturity, which could be attributed to elevated ordered stacking of aromatic units and the resulting loss of spaces within the macromolecular structure of OM. Graddock et al. (2020) also reported an increase of the BET SSA of type II kerogen until about  $R_o$  3.0% and a decreasing trend beyond  $R_o$  3.0%, although in their study, as well as in this study, data from samples with maturities above  $R_o$  3.0% are not statistically significant to support the postulate of a decreasing trend beyond  $R_o$  3.0%, mainly because a lack of economic interest in extremely high-maturity shales translates into a paucity of available data. Graphite, the ultimate fate of sedimentary OM (Weis et al., 1981),

has a BET SSA of <20 m<sup>2</sup>/g (Trammell and Pappano, 2011; Gonciaruk et al., 2021), which supports the parabolic evolutionary trend of BET SSA of OM with increasing thermal maturity. It has been reported that the BET equation may underestimate the SSA of microporous materials (Mahajan, 1991). Therefore, the low BET SSA of OM at high maturity could be partially caused by the limited application of the BET equation (Mahajan, 1991; Rouquerol et al., 2007). However, graphite has very low micropore volume and SSA (Gonciaruk et al., 2021), which suggests that the low BET SSA of OM at high maturity is real, even if it is underestimated.

Similar to the BET SSA, the Barrett-Joyner-Halenda (BJH) mesopore volume of OM also increases with increasing thermal maturity, reaches a maximum (~ 0.3 cm<sup>3</sup>/g) at  $R_o$  2.5–3.0%, and decreases with further increase of  $R_o$  (Fig. 19B). Again, there is a limited number of samples above  $R_o$  3.0% in this data set (Fig. 19B). Gonciaruk et al. (2021) reported the BJH mesopore volume of graphite to be 0.042 cm<sup>3</sup>/g, which supports the decreasing trend at higher maturities. More samples with maturities above  $R_o$  3.0% are needed to test this evolutionary trend.

Micropore characteristics characterized by Dubinin–Radushkevich (D – R) micropore surface area and Dubinin–Astakhov (D – A) micropore volume show an increase with  $R_o$  and reach ~250 m<sup>2</sup>/g and

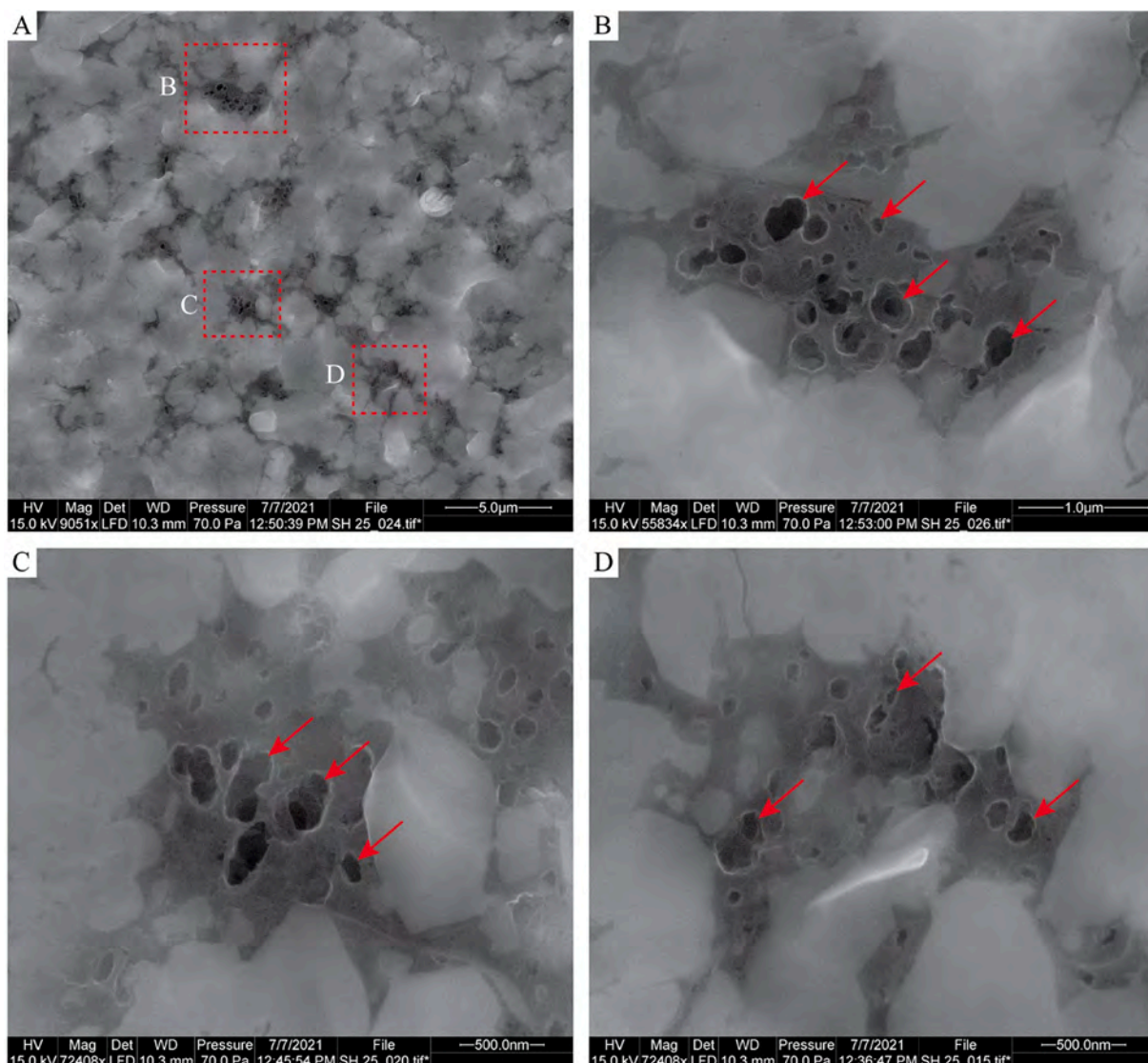


**Fig. 18.** SEM (secondary electron mode) images of organic matter (OM)-hosted pores (red arrows) in the Wufeng Formation, Sichuan Basin ( $R_o$  3.07%). OM in the images is pyrobitumen based on thermal maturity and void-filling and embayment textures. Outcrop sample of the Ordovician Wufeng Formation from Changning County, Sichuan, China. (For interpretation of the references to colour in this figure legend, the reader is referred to the web version of this article.)

$\sim 0.08 \text{ cm}^3/\text{g}$  at  $R_o$  3.0–3.5%, respectively (Fig. 19C, D). No data are available beyond  $R_o$  4.5%. However, the D – R micropore surface area and D – A micropore volume of graphite are  $8.2 \text{ m}^2/\text{g}$  and  $0.003 \text{ cm}^3/\text{g}$ , respectively (Gonciaruk et al., 2021), suggesting that OM loses most micropores at high maturity and supporting the presumed parabolic evolutionary trend of micropore characteristics with increasing thermal maturity. The maturity at which micropore properties reach maximum values ( $R_o$  3.0–3.5%) is higher than that for mesopores ( $R_o$  2.5–3.0%). This could potentially be explained by assuming that the polymerization process of OM causes an initial loss of mesopores and macropores and a subsequent loss of micropores.

One of the disadvantages of low-pressure  $N_2$  and  $CO_2$  adsorption on isolated OM from black shales is that pyrite and other heavy minerals cannot be efficiently removed during OM isolation (Vandenbroucke and Largeau, 2007). Treatment with acidic chromous chloride ( $CrCl_2$ ) under a nitrogen ( $N_2$ ) flow has been proven to be an efficient method of pyrite removal (Acholla and Orr, 1993). Another method for pyrite removal is heavy liquid separation (French et al., 2020). In the case of incomplete removal of pyrite, the measured values will be lower than the true values of OM (Liu et al., 2021) because pyrite has negligible contribution to the adsorption in low-pressure  $N_2$  and  $CO_2$  adsorption isotherms (Rexer

et al., 2014). A correction of pure OM content in isolated OM based TOC content is necessary, and then the pore structure characteristics of pure OM can be calculated based on pure OM content (not TOC content). Another disadvantage is that the dissociation of OM from the mineral matrix may expose external surfaces of OM, especially at immature and early mature stages. With the development of nanoscale pore spaces in the macromolecular structure of OM with increasing thermal maturity, the internal surface area of OM becomes significantly higher (one to several orders of magnitude; Craddock et al., 2020) than its external surface area, and the exposed external surface area could be negligible.

Coal is a good example of sedimentary rocks rich in terrigenous OM, and its pore structure can be compared with that of oil-prone OM (Fig. 19). The D – A micropore volume of coals increases with  $R_o$ , reaches a maximum ( $\sim 0.06 \text{ cm}^3/\text{g}$ ) at  $R_o \sim 4.0\%$ , and decreases afterwards (Liu et al., 2018b), exhibiting a similar evolutionary trend compared to oil-prone OM in black shales (Fig. 19D). The D – R micropore surface area of coals should follow the same trend as the D – A micropore volume. However, because of maceral variations in coals, the D – A micropore volume of coals can range from 0.01 to  $0.07 \text{ cm}^3/\text{g}$  at early maturity (Mastalerz et al., 2009; Zhao et al., 2016; Teng et al., 2017), and could potentially obscure evolutionary trends with increasing

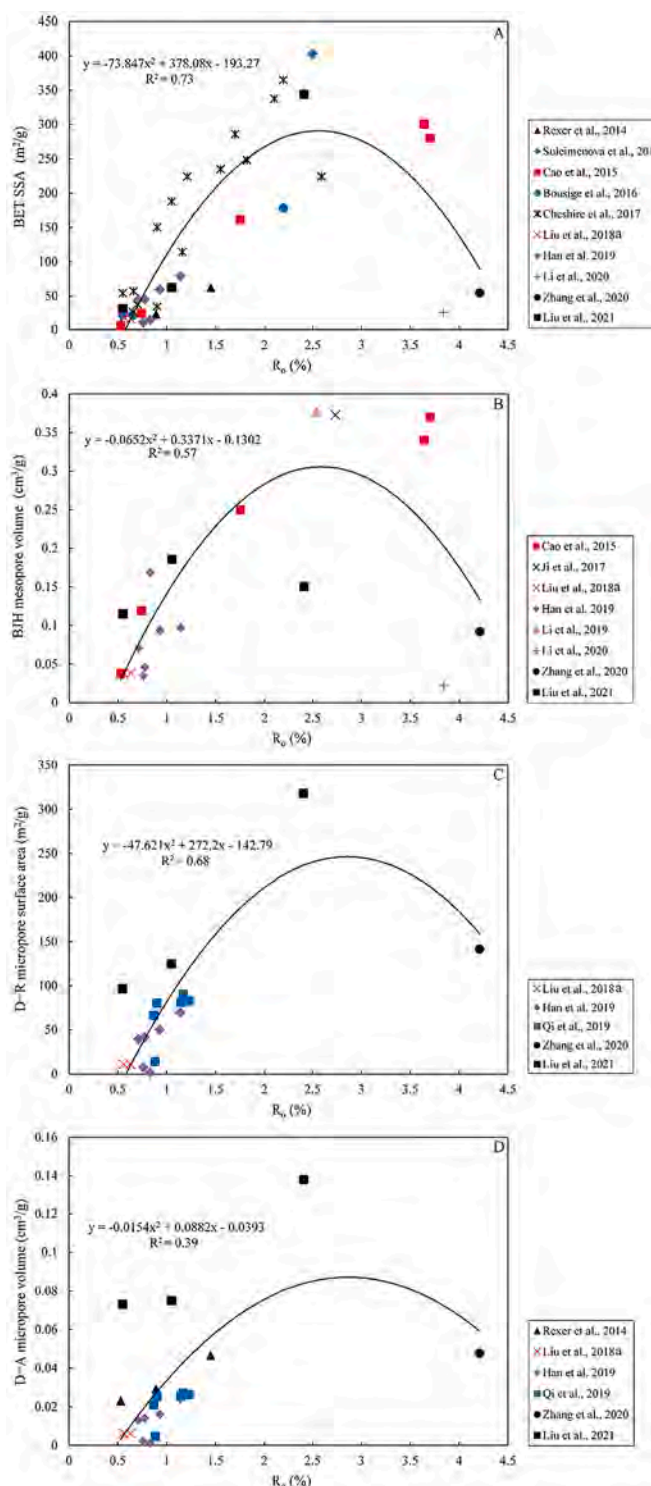


**Fig. 19.** Evolution of pore structure characteristics of isolated organic matter (OM) from black shales with increasing thermal maturity characterized by vitrinite reflectance ( $R_o$ ). (A) BET specific surface area; (B) BJH mesopore volume; (C) D – R micropore surface area; (D) D – A micropore volume.

For data from the literature, data of samples with similar depths from the same drill core were averaged and reported as the mean value. The scattering could result from inefficient removal of pyrite and other heavy minerals and heterogeneous nature of OM (sources and texture) in shales. One data point from Zhang et al. (2020) and two data points from Li et al. (2020) were omitted because are significantly off the trend, which could be caused by the above mentioned reasons.

$R_o$  values of the shale samples in Cao et al. (2015) and Qi et al. (2019) were calculated based on the empirical equation between  $R_o$  and Rock-Eval Tmax from Jarvie et al. (2001):  $R_o = 0.018 \times \text{Tmax} - 7.16$ .

BET = Brunauer–Emmett–Teller; BJH = Barrett–Joyner–Halenda; D – R = Dubinin–Radushkevich; D – A = Dubinin–Astakhov; SSA = specific surface area (Cheshire et al., 2017; Han et al., 2019; Ji et al., 2017; Li et al., 2019; Liu et al., 2018a; Suleimenova et al., 2014).

maturity.

Black shales deposited in transitional environments such as tidal and deltaic environments have high terrigenous OM input. The pore structure characteristics of bulk OM in these transitional shales should have intermediate values between oil-prone OM (Fig. 19) in shales and terrigenous OM in coals at a specific maturity. Therefore, the contribution of OM to the pore structure of shales also depends on the original OM type in addition to TOC content and thermal maturity.

Although OM has high SSA (up to 300 m<sup>2</sup>/g), its content in shales is much lower than mineral content. Clay minerals especially smectite and illite have high SSA (up to 100 m<sup>2</sup>/g; Liu et al., 2021 and references therein). The SSA of shales is controlled by OM type, content, maturity and clay minerals content and type (Liu et al., 2021). For shales that have significantly higher clay mineral content than TOC content, their SSA and methane adsorption capacity are mainly contributed by clay minerals, although OM has higher SSA and adsorption capacity per unit of mass than clays.

## 6. Summary and conclusions

In this paper, we reviewed the petrographic characteristics of major DOM in black shales under the SEM, the factors controlling the formation and preservation of OM-hosted pores, and the evolution of micropore and mesopore characteristics of OM in black shales during thermal maturation.

Organic petrographic classification of DOM is the most practical method in describing DOM in black shales because of the information on the origin of DOM. Identifying the type of DOM with confidence is a challenging task, even with an optical microscope. Correlative light and electron microscopy is so far the best approach in identifying DOM under the SEM. Accurately identifying DOM in shales with the SEM alone requires a comprehensive understanding of the studied shale formation, especially OM composition and thermal maturity.

Organic matter-hosted pores in black shales can be primary and secondary in origin. Primary organic pores are derived from the biological structure of original OM. Secondary organic pores develop during thermal maturation of oil-prone OM and are hosted by SB or pyrobitumen. Secondary organic pores are typically <1000 nm and make more contribution to the SSA and methane adsorption capacity of shales than primary organic pores. The development of secondary organic pores is controlled by thermal maturity and OM type and their preservation is controlled by thermal maturity, OM content, and mineralogical composition.

The micropore and mesopore characteristics of OM in black shales appear to follow parabolic patterns with increasing maturity characterized by R<sub>o</sub>, with an initial increase until R<sub>o</sub> 2.5–3.5% because of the development of OM-hosted pores and a subsequent decrease due to the rearrangement of the macromolecular structure of OM. We note, however, that more samples of high maturity are needed to further define this trend.

## Declaration of Competing Interest

The authors declare that they have no known competing financial interests or personal relationships that could have appeared to influence the work reported in this paper.

## Acknowledgements

This research was supported by the sponsors of the Indiana University Shale Research Consortium (Anadarko, Chevron, ConocoPhillips, ExxonMobil, Shell, Statoil, Marathon, Whiting, Wintershall). An NSF equipment grant to Juergen Schieber (EAR-0318769) provided funds for the purchase of the analytical SEM that was used for acquiring the SEM images used in this study. Bei Liu was also partially supported by the U.S. Department of Energy, Office of Science, Office of Basic Energy

Sciences, Chemical Sciences, Geosciences, and Biosciences Division under Award Number DE-SC0006978 and National Natural Science Foundation of China (Grant No. 41690131). We thank editor Dr. Shuhab Khan and reviewers Dr. Brian Cardott and Dr. Omid H. Ardakani for their constructive comments that greatly improved the quality of this paper.

## References

- Acholla, F.V., Orr, W.L., 1993. Pyrite removal from kerogen without altering organic matter: the chromous chloride method. *Energy Fuel* 7, 406–410.
- Ardakani, O.H., Sanei, H., Ghanizadeh, A., McMechan, M., Ferri, F., Clarkson, C.R., 2017. Hydrocarbon potential and reservoir characteristics of lower cretaceous Garbutt formation, Liard Basin Canada. *Fuel* 209, 274–289.
- Ardakani, O.H., Sanei, H., Ghanizadeh, A., Lavoie, D., Chen, Z., Clarkson, C.R., 2018. Do all fractions of organic matter contribute equally in shale porosity? A case study from Upper Ordovician Utica Shale, southern Quebec, Canada. *Mar. Pet. Geol.* 92, 794–808.
- Bernard, S., Horsfield, B., 2014. Thermal maturation of gas shale systems. *Annu. Rev. Earth Planet. Sci.* 42, 635–651.
- Bernard, S., Horsfield, B., Schulz, H.M., Wirth, R., Schreiber, A., Sherwood, N., 2012. Geochemical evolution of organic-rich shales with increasing maturity: a STXM and TEM study of the Posidonia Shale (lower Toarcian, northern Germany). *Mar. Pet. Geol.* 31, 70–89.
- Bertrand, R., 1990. Correlations among the reflectances of vitrinite, chitinozoans, graptolites and scolecodonts. *Org. Geochem.* 15, 565–574.
- Bertrand, R., Héroux, Y., 1987. Chitinozoan, graptolite, and scolecodont reflectance as an alternative to vitrinite and pyrobitumen reflectance in Ordovician and Silurian strata, Anticosti Island, Quebec, Canada. *AAPG Bull.* 71, 951–957.
- Bousige, C., Ghimbeu, C.M., Vix-Guterl, C., Pomerantz, A.E., Suleimanova, A., Vaughan, G., Garbarino, G., Feygenson, M., Wildgruber, C., Ulm, F.-J., Pellenq, R.J.-M., Coasne, B., 2016. Realistic molecular model of kerogen's nanostructure. *Nat. Mater.* 15, 576–582.
- Buchardt, B., Lewan, M.D., 1990. Reflectance of vitrinite-like macerals as a thermal maturity index for Cambrian-Ordovician Alum Shale, southern Scandinavia. *AAPG Bull.* 74, 394–406.
- Bustin, R.M., Link, C., Goodarzi, F., 1989. Optical properties and chemistry of graptolite periderm following laboratory simulated maturation. *Org. Geochem.* 14, 355–364.
- Camp, W.K., 2016. Strategies for identifying organic matter types in SEM. In: AAPG Search and Discovery Article No. 70233.
- Camp, W., 2019. Diagenetic evolution of organic matter cements: Implications for unconventional shale reservoir quality prediction. In: Camp, W., Milliken, K., Taylor, K., Fishman, N., Hackley, P., Macquaker, J. (Eds.), Mudstone Diagenesis: Research Perspectives for Shale Hydrocarbon Reservoirs, Seals, and Source Rocks, AAPG Memoir, vol. 120, pp. 209–224.
- Canter, L., Zhang, S., Sonnenfeld, M., Bugge, C., Guisinger, M., Jones, K., 2016. Primary and secondary organic matter habit in unconventional reservoirs. In: Olson, T. (Ed.), Imaging Unconventional Reservoir Pore Systems, AAPG Memoir, vol. 112, pp. 9–23.
- Cao, T., Song, Z., Wang, S., Xia, J., 2015. A comparative study of the specific surface area and pore structure of different shales and their kerogens. *Sci. China Earth Sci.* 58, 510–522.
- Cardott, B.J., Curtis, M.E., 2018. Identification and nanoporosity of macerals in coal by scanning electron microscopy. *Int. J. Coal Geol.* 190, 205–217.
- Cardott, B.J., Landis, C.R., Curtis, M.E., 2015. Post-oil solid bitumen network in the Woodford Shale, USA—A potential primary migration pathway. *Int. J. Coal Geol.* 139, 106–113.
- Cheshire, S., Craddock, P.R., Xu, G., Sauerer, B., Pomerantz, A.E., McCormick, D., Abdallah, W., 2017. Assessing thermal maturity beyond the reaches of vitrinite reflectance and Rock-Eval pyrolysis: a case study from the Silurian Qusaiba formation. *Int. J. Coal Geol.* 180, 29–45.
- Craddock, P.R., Haecker, A., Bake, K.D., Pomerantz, A.E., 2020. Universal curves describing the chemical and physical evolution of type II kerogen during thermal maturation. *Energy Fuel* 34, 15217–15233.
- Curtis, J.B., 2002. Fractured shale-gas systems. *AAPG Bull.* 86, 1921–1938.
- Curtis, M.E., Ambrose, R.J., Sondergeld, C.H., Rai, C.S., 2011. Transmission and scanning electron microscopy investigation of pore connectivity of gas shales on the nanoscale. In: North American Unconventional Gas Conference and Exhibition. Society of Petroleum Engineers, The Woodlands, Texas, USA, June 14–16, 2011, 144391. SPE (10 p).
- Curtis, M.E., Cardott, B.J., Sondergeld, C.H., Rai, C.S., 2012. Development of organic porosity in the Woodford Shale with increasing thermal maturity. *Int. J. Coal Geol.* 103, 26–31.
- Dong, T., Harris, N.B., 2020. The effect of thermal maturity on porosity development in the Upper Devonian–lower Mississippian Woodford Shale, Permian Basin, US: Insights into the role of silica nanospheres and microcrystalline quartz on porosity preservation. *Int. J. Coal Geol.* 217, 103346.
- Dong, T., Harris, N.B., McMillan, J.M., Twemlow, C.E., Nassichuk, B.R., Bish, D.L., 2019. A model for porosity evolution in shale reservoirs: an example from the Upper Devonian Duvernay formation, Western Canada sedimentary basin. *AAPG Bull.* 103, 1017–1044.
- Durand, B., 1980. Sedimentary organic matter and kerogen: Definition and quantitative importance of kerogen. In: Durand, B. (Ed.), Kerogen: Insoluble Organic Matter from Sedimentary Rocks. Editions Technip, Paris, pp. 13–34.

- Fishman, N.S., Hackley, P.C., Lowers, H.A., Hill, R.J., Egenhoff, S.O., Eberl, D.D., Blum, A.E., 2012. The nature of porosity in organic-rich mudstones of the Upper Jurassic Kimmeridge Clay Formation, North Sea, offshore United Kingdom. *Int. J. Coal Geol.* 103, 32–50.
- Flores, D., Suárez-Ruiz, I., 2017. Organic petrology in the study of dispersed organic matter. In: Suárez-Ruiz, I., Filho, J.G.M. (Eds.), *The Role of Organic Petrology in the Exploration of Conventional and Unconventional Hydrocarbon Systems*. Bentham Science Publishers, Sharjah, pp. 34–76.
- French, K.L., Birdwell, J.E., Lewan, M.D., 2020. Trends in thermal maturity indicators for the organic sulfur-rich Eagle Ford Shale. *Mar. Pet. Geol.* 118, 104459.
- Gonciaruk, A., Hall, M.R., Fay, M.W., Parmenter, C.D., Vane, C.H., Khlobystov, A.N., Ripepi, N., 2021. Kerogen nanoscale structure and CO<sub>2</sub> adsorption in shale micropores. *Sci. Report.* 11, 1–13.
- Gong, J., Qiu, Z., Zou, C., Wang, H., Shi, Z., 2020. An integrated assessment system for shale gas resources associated with graptolites and its application. *Appl. Energy* 262, 114524.
- Goodarzi, F., Norford, B.S., 1989. Variation of graptolite reflectance with depth of burial. *Int. J. Coal Geol.* 11, 127–141.
- Hackley, P.C., Cardott, B.J., 2016. Application of organic petrography in north American shale petroleum systems: a review. *Int. J. Coal Geol.* 163, 8–51.
- Hackley, P.C., Lewan, M., 2018. Understanding and distinguishing reflectance measurements of solid bitumen and vitrinite using hydrolytic pyrolysis: Implications to petroleum assessment. *AAPG Bull.* 102, 1119–1140.
- Hackley, P.C., Valentine, B.J., Voortman, L.M., Van Oosten Slingeland, D.S.B., Hatcherian, J., 2017. Utilization of integrated correlative light and electron microscopy (ICLEM) for imaging sedimentary organic matter. *J. Microsc.* 267, 371–383.
- Hackley, P.C., Valentine, B.J., Hatcherian, J.J., 2018. On the petrographic distinction of bituminite from solid bitumen in immature to early mature source rocks. *Int. J. Coal Geol.* 196, 232–245.
- Hackley, P.C., Jubb, A.M., McAleer, R.J., Valentine, B.J., Birdwell, J.E., 2021. A review of spatially resolved techniques and applications of organic petrography in shale petroleum systems. *Int. J. Coal Geol.* 241, 103745.
- Han, H., Pang, P., Li, Z.L., Shi, P.T., Guo, C., Liu, Y., Chen, S.J., Lu, J.G., Gao, Y., 2019. Controls of organic and inorganic compositions on pore structure of lacustrine shales of Chang 7 member from Triassic Yanchang Formation in the Ordos Basin, China. *Mar. Pet. Geol.* 100, 270–284.
- Hao, F., Zou, H., Lu, Y., 2013. Mechanisms of shale gas storage: Implications for shale gas exploration in China. *AAPG Bull.* 97, 1325–1346.
- Inan, S., Al Badairi, H., İnan, T., Al Zahrani, A., 2018. Formation and occurrence of organic matter-hosted porosity in shales. *Int. J. Coal Geol.* 199, 39–51.
- International Committee for Coal Petrology (ICCP), 1998. The new vitrinite classification (ICCP System 1994). *Fuel* 77, 349–358.
- International Committee for Coal Petrology (ICCP), 2001. The new inertinite classification (ICCP System 1994). *Fuel* 80, 459–471.
- Jacob, H., 1989. Classification, structure, genesis and practical importance of natural solid oil bitumen ("migrabitumen"). *Int. J. Coal Geol.* 11, 65–79.
- Jarvie, D.M., 2012a. Shale resource systems for oil and gas: Part 1—Shale-gas resource systems. In: Breyer, J.A. (Ed.), *Shale Reservoirs—Giant Resources for the 21st Century*. AAPG Memoir, vol. 97, pp. 69–87.
- Jarvie, D.M., 2012b. Shale resource systems for oil and gas: Part 1—Shale-oil resource systems. In: Breyer, J.A. (Ed.), *Shale Reservoirs—Giant Resources for the 21st Century*. AAPG Memoir, vol. 97, pp. 89–119.
- Jarvie, D.M., Claxton, B.L., Henk, F., Breyer, J.T., 2001. Oil and shale gas from the Barnett Shale, Fort Worth Basin, Texas. In: *AAPG Annual Meeting Program*, 10, p. A100.
- Jarvie, D.M., Hill, R.J., Ruble, T.E., Pollastro, R.M., 2007. Unconventional shale-gas systems: the Mississippian Barnett Shale of north-Central Texas as one model for thermogenic shale-gas assessment. *AAPG Bull.* 91, 475–499.
- Ji, W., Song, Y., Rui, Z., Meng, M., Huang, H., 2017. Pore characterization of isolated organic matter from high matured gas shale reservoir. *Int. J. Coal Geol.* 174, 31–40.
- Katz, B.J., Arango, I., 2018. Organic porosity: a geochemist's view of the current state of understanding. *Org. Geochem.* 123, 1–16.
- Kenrick, P., Crane, P.R., 1997. The origin and early evolution of plants on land. *Nature* 389, 33–39.
- Knapp, L.J., Ardakani, O.H., Uchida, S., Nanjo, T., Otomo, C., Hattori, T., 2020. The influence of rigid matrix minerals on organic porosity and pore size in shale reservoirs: Upper Devonian Duvernay Formation, Alberta, Canada. *Int. J. Coal Geol.* 227, 103525.
- Ko, L.T., Ruppel, S.C., Loucks, R.G., Hackley, P.C., Zhang, T., Shao, D., 2018. Pore-types and pore-network evolution in Upper Devonian-lower Mississippian Woodford and Mississippian Barnett mudstones: Insights from laboratory thermal maturation and organic petrology. *Int. J. Coal Geol.* 190, 3–28.
- Kus, J., Araujo, C.V., Borrego, A.G., Flores, D., Hackley, P.C., Hámor-Vidó, M., Kalaitzidis, S., Kommeren, C.J., Kwiecińska, B., Mastalerz, M., Mendonça Filho, J.G., Menezes, T.R., Misz-Kennan, M., Nowak, G.J., Petersen, H.I., Rallakis, D., Suárez-Ruiz, I., Sýkorová, I., Životíć, D., 2017. Identification of alginite and bituminite in rocks other than coal. 2006, 2009, and 2011 round robin exercises of the ICCP Identification of Dispersed Organic Matter Working Group. *Int. J. Coal Geol.* 178, 26–38.
- Kwiecińska, B., Pusz, S., Valentine, B.J., 2019. Application of electron microscopy TEM and SEM for analysis of coals, organic-rich shales and carbonaceous matter. *Int. J. Coal Geol.* 211, 103203.
- Landis, C.R., Castaño, J.R., 1995. Maturation and bulk chemical properties of a suite of solid hydrocarbons. *Org. Geochem.* 22, 137–149.
- Li, Z., Jiang, Z., Yu, H., Liang, Z., 2019. Organic matter pore characterization of the Wufeng-Longmaxi shales from the fuling gas field, Sichuan Basin: evidence from organic matter isolation and low-pressure CO<sub>2</sub> and N<sub>2</sub> adsorption. *Energies* 12, 1027.
- Li, X., Jiang, Z., Jiang, S., Li, Z., Song, Y., Jiang, H., Qiu, H., Cao, X., Miao, Y., 2020. Various controlling factors of matrix-related pores from differing depositional shales of the Yangtze Block in South China: Insight from organic matter isolation and fractal analysis. *Mar. Pet. Geol.* 111, 720–734.
- Liu, K., Ostadhassan, M., Zou, J., Gentzis, T., Rezaee, R., Bubach, B., Carvajal-Ortiz, H., 2018a. Nanopore structures of isolated kerogen and bulk shale in Bakken formation. *Fuel* 226, 441–453.
- Liu, Y., Zhu, Y., Liu, S., Chen, S., Li, W., Wang, Y., 2018b. Molecular structure controls on micropore evolution in coal vitrinite during coalification. *Int. J. Coal Geol.* 199, 19–30.
- Liu, B., Schieber, J., Mastalerz, M., 2019a. Petrographic and micro-FTIR study of organic matter in the Upper Devonian New Albany Shale during thermal maturation: Implications for kerogen transformation. In: Camp, W., Milliken, K., Taylor, K., Fishman, N., Hackley, P., Macquaker, J. (Eds.), *Mudstone Diagenesis: Research Perspectives for Shale Hydrocarbon Reservoirs, Seals, and Source Rocks*, AAPG Memoir, vol. 120, pp. 165–188.
- Liu, B., Schieber, J., Mastalerz, M., Teng, J., 2019b. Organic matter content and type variation in the sequence stratigraphic context of the Upper Devonian New Albany Shale, Illinois Basin. *Sediment. Geol.* 383, 101–120.
- Liu, B., Mastalerz, M., Schieber, J., Teng, J., 2020a. Association of uranium with macerals in marine black shales: Insights from the Upper Devonian New Albany Shale, Illinois Basin. *Int. J. Coal Geol.* 217, 103351.
- Liu, B., Teng, J., Mastalerz, M., Schieber, J., 2020b. Assessing the thermal maturity of black shales using vitrinite reflectance: Insights from Devonian black shales in the eastern United States. *Int. J. Coal Geol.* 220, 103426.
- Liu, B., Teng, J., Mastalerz, M., Schieber, J., Schimmelmann, A., Bish, D., 2021. Compositional control on shale pore structure characteristics across a maturation gradient: Insights from the Devonian New Albany Shale and Marcellus Shale in the eastern United States. *Energy Fuel* 35, 7913–7929.
- Liu, B., Schieber, J., Mastalerz, M., 2017. Combined SEM and reflected light petrography of organic matter in the New Albany Shale (Devonian-Mississippian) in the Illinois Basin: a perspective on organic pore development with thermal maturation. *Int. J. Coal Geol.* 184, 57–72.
- Löhr, S.C., Baruch, E.T., Hall, P.A., Kennedy, M.J., 2015. Is organic pore development in gas shales influenced by the primary porosity and structure of thermally immature organic matter? *Org. Geochem.* 87, 119–132.
- Loucks, R.G., Reed, R.M., 2014. Scanning-electron-microscope petrographic evidence for distinguishing organic-matter pores associated with depositional organic matter versus migrated organic matter in mudrocks. *Gulf Coast Assoc. Geol. Soc. J.* 3, 51–60.
- Loucks, R.G., Reed, R.M., Ruppel, S.C., Jarvie, D.M., 2009. Morphology, genesis, and distribution of nanometer-scale pores in siliceous mudstones of the Mississippian Barnett Shale. *J. Sediment. Res.* 79, 848–861.
- Loucks, R.G., Reed, R.M., Ruppel, S.C., Hammes, U., 2012. Spectrum of pore types and networks in mudrocks and a descriptive classification for matrix-related mudrock pores. *AAPG Bull.* 96, 1071–1098.
- Luo, Q., Zhong, N., Dai, N., Zhang, W., 2016. Graptolite-derived organic matter in the Wufeng-Longmaxi formations (Upper Ordovician–lower Silurian) of southeastern Chongqing, China: Implications for gas shale evaluation. *Int. J. Coal Geol.* 153, 87–98.
- Luo, Q., Hao, J., Skovsted, C.B., Luo, P., Khan, I., Wu, J., Zhong, N., 2017. The organic petrology of graptolites and maturity assessment of the Wufeng-Longmaxi Formations from Chongqing, China: Insights from reflectance cross-plot analysis. *Int. J. Coal Geol.* 183, 161–173.
- Luo, Q., Fariborz, G., Zhong, N., Wang, Y., Qiu, N., Skovsted, C.B., Suchý, V., Schovsbo, N.H., Morga, R., Xu, Y., Hao, J., Liu, A., Wu, J., Cao, W., Min, X., Wu, J., 2020. Graptolites as fossil geo-thermometers and source material of hydrocarbons: an overview of four decades of progress. *Earth Sci. Rev.* 200, 103000.
- Ma, Y., Zhong, N., Cheng, L., Pan, Z., Dai, N., Zhang, Y., Yang, L., 2016. Pore structure of the graptolite-derived OM in the Longmaxi Shale, southeastern Upper Yangtze Region, China. *Mar. Pet. Geol.* 72, 1–11.
- Ma, Y., Ardakani, O.H., Zhong, N., Liu, H., Huang, H., Larter, S., Zhang, C., 2020. Possible pore structure deformation effects on the shale gas enrichment: an example from the lower Cambrian shales of the Eastern Upper Yangtze Platform, South China. *Int. J. Coal Geol.* 217, 103349.
- Mahajan, O.P., 1991. CO<sub>2</sub> surface area of coals: the 25-year paradox. *Carbon* 29, 735–742.
- Mastalerz, M., Schieber, J., 2017. Effect of ion milling on the perceived maturity of shale samples: implications for organic petrography and SEM analysis. *Int. J. Coal Geol.* 183, 110–119.
- Mastalerz, M., Drobniak, A., Schimmelmann, A., 2009. Changes in optical properties, chemistry, and micropore and mesopore characteristics of bituminous coal at the contact with dikes in the Illinois Basin. *Int. J. Coal Geol.* 77, 310–319.
- Mastalerz, M., Schimmelmann, A., Lis, G.P., Drobniak, A., Stankiewicz, A., 2012. Influence of maceral composition on geochemical characteristics of immature shale kerogen: Insight from density fraction analysis. *Int. J. Coal Geol.* 103, 60–69.
- Mastalerz, M., Schimmelmann, A., Drobniak, A., Chen, Y., 2013. Porosity of Devonian and Mississippian New Albany Shale across a maturation gradient: Insights from organic petrology, gas adsorption, and mercury intrusion. *AAPG Bull.* 97, 1621–1643.
- Mastalerz, M., Karayigit, A., Hampton, L., Drobniak, A., 2016a. Variations in gas content in organic matter-rich low maturity shale; example from the New Albany Shale in the Illinois Basin. *J. Pet. Nat. Gas* 1, 1–16.

- Mastalerz, M., Drobniak, A., Meyer, R., 2016b. Atlas of New Albany Shale photomicrographs of organic matter. Indiana Geol. Surv. Digit. Inform. Ser. 3. <https://igws.indiana.edu/IGSMap/NASPhotomicro>.
- Mastalerz, M., Drobniak, A., Stankiewicz, A.B., 2018. Origin, properties, and implications of solid bitumen in source-rock reservoirs: a review. *Int. J. Coal Geol.* 195, 14–36.
- McCartney, J.T., Teichmüller, M., 1972. Classification of coals according to degree of coalification by reflectance of the vitrinite component. *Fuel* 51, 64–68.
- Milliken, K.L., Rudnicki, M., Awwiller, D.N., Zhang, T., 2013. Organic matter-hosted pore system, Marcellus formation (Devonian), Pennsylvania. *AAPG Bull.* 97, 177–200.
- Milliken, K.L., Ko, L.T., Pommer, M., Marsaglia, K.M., 2014. SEM petrography of Eastern Mediterranean sapropels: Analogue data for assessing organic matter in oil and gas shales. *J. Sediment. Res.* 84, 961–974.
- Mukhopadhyay, P.K., 1994. Vitrinite reflectance as a maturity parameter: Petrographic and molecular characterization and its applications to basin modeling. In: Mukhopadhyay, P.K., Dow, W.G. (Eds.), *Vitrinite Reflectance as A Maturity Parameter: Applications and Limitations*, pp. 1–24.
- O'Brien, N.R., Thyne, G.D., Slatt, R.M., 1996. Morphology of hydrocarbon droplets during migration: Visual example from the Monterey Formation (Miocene), California. *AAPG Bull.* 80, 1710–1718.
- Passey, Q.R., Bohacs, K.M., Esch, W.L., Klimentidis, R., Sinha, S., 2010. From oil-prone source rock to gas-producing shale reservoir-geologic and petrophysical characterization of unconventional shale-gas reservoirs. In: Chinese Petroleum Society/Society of Petroleum Engineers International Oil and Gas Conference and Exhibition, Beijing, China, June 8–10, 2010, 131350. SPE (29 p).
- Peters, K.E., Cassa, M.R., 1994. Applied source rock geochemistry. In: Magoon, L.B., Dow, W.G. (Eds.), *The Petroleum System—From Source to Trap*, AAPG Memoir, vol. 60, pp. 93–120.
- Petersen, H.I., Schovbo, N.H., Nielsen, A.T., 2013. Reflectance measurements of zooclasts and solid bitumen in lower Paleozoic shales, southern Scandinavia: Correlation to vitrinite reflectance. *Int. J. Coal Geol.* 114, 1–18.
- Pickel, W., Kus, J., Flores, D., Kalaitzidis, S., Christanis, K., Cardott, B.J., Miszkiewicz, M., Rodrigues, S., Hentschel, A., Hamor-Vido, M., Crosdale, P., Wagner, N., ICCP, 2017. Classification of liptinite-ICCP system 1994. *Int. J. Coal Geol.* 169, 40–61.
- Potter, J., Stasiuk, L.D., Cameron, A.R., 1998. A petrographic atlas of Canadian coal macerals and dispersed organic matter. In: Canadian Society for Coal Science and Organic Petrology—Geological Survey of Canada (Calgary)-Canmet Energy Technology Centre (105 p).
- Qiu, Y., Ju, Y., Huang, C., Zhu, H., Bao, Y., Wu, J., Meng, S., Chen, W., 2019. Influences of organic matter and kaolinite on pore structures of transitional organic-rich mudstone with an emphasis on  $S_2$  controlling specific surface area. *Fuel* 237, 860–873.
- Qiu, Z., Zou, C., 2020. Controlling factors on the formation and distribution of “sweet-spot areas” of marine gas shales in South China and a preliminary discussion on unconventional petroleum sedimentology. *J. Asian Earth Sci.* 194, 103989.
- Qiu, Z., Zou, C., Li, X., Wang, H., Dong, D., Lu, B., Zhou, S., Shi, Z., Feng, Z., Zhang, M., 2018. Discussion on the contribution of graptolite to organic enrichment and gas shale reservoir: a case study of the Wufeng-Longmaxi shales in South China. *J. Nat. Gas Geosci.* 3, 147–156.
- Qiu, Z., Zou, C., Wang, H., Dong, D., Lu, B., Chen, Z., Liu, D., Li, G., Liu, H., He, J., Wei, L., 2020a. Discussion on the characteristics and controlling factors of differential enrichment of shale gas in the Wufeng-Longmaxi formations in South China. *J. Nat. Gas Geosci.* 5, 117–128.
- Qiu, Z., Liu, B., Dong, D., Lu, B., Yawar, Z., Chen, Z., Schieber, J., 2020b. Silica diagenesis in the lower Paleozoic Wufeng and Longmaxi formations in the Sichuan Basin, South China: Implications for reservoir properties and paleoproductivity. *Mar. Pet. Geol.* 121, 104594.
- Qiu, Z., Liu, B., Lu, B., Shi, Z., Li, Z., 2022. Mineralogical and petrographic characteristics of the Ordovician-Silurian Wufeng-Longmaxi Shale in the Sichuan Basin and implications for depositional conditions and diagenesis of black shales. *Mar. Pet. Geol.* 135, 105428.
- Reed, R.M., Loucks, R.G., Ko, L.T., 2020. SEM petrographic differentiation among different types of pores associated with organic matter in mudrocks. *Gulf Coast Assoc. Geol. Soc. J.* 9, 17–27.
- Rexer, T.F., Mathia, E.J., Aplin, A.C., Thomas, K.M., 2014. High-pressure methane adsorption and characterization of pores in *Posidonia* shales and isolated kerogens. *Energy Fuel* 28, 2886–2901.
- Reyes, J., Jiang, C., Lavoie, D., Armstrong, D.K., Milovic, M., Robinson, R., 2018. Organic petrographic analysis of artificially matured chitinozoan-and graptolite-rich Upper Ordovician shale from Hudson Bay Basin, Canada. *Int. J. Coal Geol.* 199, 138–151.
- Ross, D.J.K., Bustin, R.M., 2009. The importance of shale composition and pore structure upon gas storage potential of shale gas reservoirs. *Mar. Pet. Geol.* 26, 916–927.
- Rouquerol, J., Avnir, D., Fairbridge, C.W., Everett, D.H., Haynes, J.M., Pernicone, N., Ramsay, J.D.F., Sing, K.S.W., Unger, K.K., 1994. Recommendations for the characterization of porous solids (Technical Report). *Pure Appl. Chem.* 66, 1739–1758.
- Rouquerol, J., Llewellyn, P., Rouquerol, F., 2007. Is the BET equation applicable to microporous adsorbents? In: Llewellyn, P., Rodriguez-Reinoso, F., Rouquerol, J., Seaton, N., (Eds.). *Stud. Surf. Sci. Catal.* 160, 49–56.
- Sanei, H., 2020. Genesis of solid bitumen. *Sci. Rep.* 10, 1–10.
- Schieber, J., 2010. Common themes in the formation and preservation of intrinsic porosity in shales and mudstones—illustrated with examples across the Phanerozoic. In: *SPE Unconventional Gas Conference*. Society of Petroleum Engineers, Pittsburgh, Pennsylvania, USA, February 23–25, 2010. SPE, p. 132370 (10 p).
- Schieber, J., 2013. SEM observations on ion-milled samples of Devonian black shales from Indiana and New York: The petrographic context of multiple pore types. In: Camp, W., Diaz, E., Wawak, B. (Eds.), *Electron Microscopy of Shale Hydrocarbon Reservoirs*, AAPG Memoir, vol. 102, pp. 153–171.
- Schieber, J., Lazar, R., Bohacs, K., Klimentidis, R., Dumitrescu, M., Ottmann, J., 2016. An SEM study of porosity in the Eagle Ford Shale of Texas—Pore types and porosity distribution in a depositional and sequence-stratigraphic Context. In: Breyer, J.A. (Ed.), *The Eagle Ford Shale: A Renaissance in U.S. Oil Production*. AAPG Memoir, vol. 110, pp. 167–186.
- Schleicher, M., Koster, J., Kulke, H., Weil, W., 1998. Reservoir and source-rock characterisation of the early Palaeozoic interval in the Peribaltic Syncline, northern Poland. *J. Pet. Geol.* 21, 33–56.
- Schmidt, J.S., Menezes, T.R., Souza, I.V.A.F., Spigolon, A.L.D., Pestilho, A.L.S., Coutinho, L.F.C., 2019. Comments on empirical conversion of solid bitumen reflectance for thermal maturity evaluation. *Int. J. Coal Geol.* 201, 44–50.
- Schoenherr, J., Little, R., Urai, J.L., Kukla, P.A., Rawahi, Z., 2007. Polyphase thermal evolution in the Infra-Cambrian Ara Group (South Oman Salt Basin) as deduced by maturity of solid reservoir bitumen. *Org. Geochem.* 38, 1293–1318.
- Senftle, J.T., Brown, J.H., Carter, S.R., 1987. Refinement of organic petrographic methods for kerogen characterization. *Int. J. Coal Geol.* 7, 105–117.
- Stasiuk, I.D., Burgess, J., Thompson-Rizer, C., Hutton, A., Cardott, B., 2002. Status report on TSOP-ICCP dispersed organic matter classification working group. *Soc. Org. Petrol. Newslett.* 19 (3), 14.
- Strapoć, D., Mastalerz, M., Schimmelmann, A., Drobniak, A., Hasenmueller, N.R., 2010. Geochemical constraints on the origin and volume of gas in the New Albany Shale (Devonian–Mississippian), eastern Illinois Basin. *AAPG Bull.* 94, 1713–1740.
- Suárez-Ruiz, I., Flores, D., Mendonça Filho, J.G., Hackley, P.C., 2012. Review and update of the applications of organic petrology: part 1, geological applications. *Int. J. Coal Geol.* 99, 54–112.
- Suleimenova, A., Bake, K.D., Ozkan, A., Valenza II, J.J., Kleinberg, R.L., Burnham, A.K., Ferralis, N., Pomerantz, A.E., 2014. Acid demineralization with critical point drying: a method for kerogen isolation that preserves microstructure. *Fuel* 135, 492–497.
- Taylor, G.H., Teichmüller, M., Davis, A., Diessel, C.F.K., Little, R., Robert, P., 1998. *Organic Petrology*. Gebrüder Borntraeger, Berlin-Stuttgart (704 p).
- Teng, J., Mastalerz, M., Hampton, L., 2017. Maceral controls on porosity characteristics of lithotypes of Pennsylvanian high volatile bituminous coal: example from the Illinois Basin. *Int. J. Coal Geol.* 172, 80–94.
- Teng, J., Mastalerz, M., Liu, B., 2021. Petrographic and chemical structure characteristics of amorphous organic matter in marine black shales: Insights from Pennsylvanian and Devonian black shales in the Illinois Basin. *Int. J. Coal Geol.* 235, 103676.
- Tenger, B., Lu, L., Yu, L., Zhang, W., Pan, A., Shen, B., Wang, Y., Yang, Y., Gao, Z., 2021. Formation, preservation and connectivity control of organic pores in shale. *Pet. Explor. Dev.* 48, 687–699.
- Thompson, C.L., Dembicki Jr., H., 1986. Optical characteristics of amorphous kerogens and the hydrocarbon-generating potential of source rocks. *Int. J. Coal Geol.* 6, 229–249.
- Tissot, B.P., Welte, D.H., 1984. *Petroleum Formation and Occurrence*, 2nd ed. Springer-Verlag, Berlin. (699 p).
- Trammell, M.P., Pappano, P.J., 2011. Analysis of Natural Graphite, Synthetic Graphite, and Thermosetting Resin Candidates for Use in Fuel Compact Matrix. Oak Ridge National Laboratory, Oak Ridge, TN, ORNL/TM-2011/315. <https://doi.org/10.2172/1024284>, 66 p.
- Tricker, P.M., Marshall, J.E., Badman, T.D., 1992. Chitinozoan reflectance: a lower Palaeozoic thermal maturity indicator. *Mar. Pet. Geol.* 9, 302–307.
- Valentine, B.J., Hackley, P.C., 2019. Applications of correlative light and electron microscopy (CLEM) to organic matter in the north American shale petroleum systems. In: Camp, W., Milliken, K., Taylor, K., Fishman, N., Hackley, P., Macquaker, J. (Eds.), *Mudstone Diagenesis: Research Perspectives for Shale Hydrocarbon Reservoirs, Seals, and Source Rocks*, AAPG Memoir, vol. 120, pp. 1–17.
- Valentine, B.J., Hackley, P.C., Hatcherian, J., Yu, J.J., 2019. Reflectance increase from broad beam ion milling of coals and organic-rich shales due to increased surface flatness. *Int. J. Coal Geol.* 201, 86–101.
- Vandenbroucke, M., Largeau, C., 2007. Kerogen origin, evolution and structure. *Org. Geochem.* 38 (5), 719–833.
- Wang, F.P., Reed, R.M., John, A., Katherine, G., 2009. Pore networks and fluid flow in gas shales. In: *SPE Annual Technical Conference and Exhibition*. Society of Petroleum Engineers, New Orleans, Louisiana, USA, October 4–7, 2009, 124253. SPE (8 p).
- Wei, L., Sun, S., Dong, D., Shi, Z., Yin, J., Zhang, S., Mastalerz, M., Cheng, X., 2021. Petrographic characterization and maceral controls on porosity in overmature marine shales: examples from Ordovician-Silurian shales in China and the US. *Geofluids* 2021, 5582262.
- Weis, P.L., Friedman, I., Gleason, J.P., 1981. The origin of epigenetic graphite: evidence from isotopes. *Geochim. Cosmochim. Acta* 45, 2325–2332.
- Wu, Z., He, S., Han, Y., Zhai, G., He, X., Zhou, Z., 2020. Effect of organic matter type and maturity on organic matter pore formation of transitional facies shales: a case study on Upper Permian Longtan and Dalong Shales in middle Yangtze region, China. *J. Earth Sci.* 31, 368–384.

- Yang, C., Xiong, Y., Zhang, J., 2020. A comprehensive re-understanding of the OM-hosted nanopores in the marine Wufeng–Longmaxi shale formation in South China by organic petrology, gas adsorption, and X-ray diffraction studies. *Int. J. Coal Geol.* 218, 103362.
- Zhang, H., Li, X., Hao, Q., He, D., Zhuang, J., 2003. Scanning Electron Microscopic Study of Coal in China. Geological Publishing House, Beijing, pp. 70–71 (In Chinese).
- Zhang, Y., Yu, B., Pan, Z., Hou, C., Zuo, Q., Sun, M., 2020. Effect of thermal maturity on shale pore structure: a combined study using extracted organic matter and bulk shale from Sichuan Basin, China. *J. Nat. Gas Sci. Eng.* 74, 103089.
- Zhao, J., Xu, H., Tang, D., Mathews, J.P., Li, S., Tao, S., 2016. A comparative evaluation of coal specific surface area by CO<sub>2</sub> and N<sub>2</sub> adsorption and its influence on CH<sub>4</sub> adsorption capacity at different pore sizes. *Fuel* 183, 420–431.
- Zheng, X., Sanei, H., Schovsbo, N.H., Luo, Q., Wu, J., Zhong, N., Galloway, J.M., Goodarzi, F., 2021. Role of zooclasts in the kerogen type and hydrocarbon potential of the lower Paleozoic Alum Shale. *Int. J. Coal Geol.* 248, 103865.